OPTICAL REFRIGERATION UNDER LASER AND SOLAR IRRADIATION

by

Surya Prakash Seshaiya Doraiswamy Chandrasekar

in partial fulfilment of the requirements for the degree of

Master of Science
in Mechanical Engineering, Track: Sustainable Process and Energy Technology

at the Delft University of Technology,
to be defended publicly on Wednesday July 11, 2018 at 14:00 PM.

Student number:	4516885	
P&E report number:	2893	
Project duration:	July 1,2017 – July 11, 2018	
Thesis committee:	Prof.dr. Dirk Roekaerts,	TU Delft, supervisor
	Prof.dr. Peter Steeneken,	TU Delft
	Dr. Aurele Adam	TU Delft
	Dr. Daniel Irimia	TU Delft

EMBARGO

- *The graduation project of Mr. Surya Prakash Seshaiya Doraiswamy Chandrasekar has been initiated without the involvement of any existing company.*

- *The project was initiated based on innovative ideas on unconventional optical refrigeration proposed solely by the graduating student.*

- *With the help of TU Delft, the student aims to submit an STW valorization grant proposal in order to take this novel technological solution into business.*

- *To protect the intellectual property rights of the author, this report is under embargo between June 27th, 2018 and June 27th, 2023.*

ABSTRACT

The concept of optical refrigeration dates back to 1929, when Pringsheim recognized that thermal energy associated with the translational degrees of freedom of isolated atoms could be reduced by the process of anti-Stokes fluorescence. Optical refrigeration of a solid was first experimentally demonstrated in 1995 with the Ytterbium-doped fluorozirconate glass by Epstein and his team and since then this invigorating field has garnered much scientific interest for development of an all optical refrigerator. The present works discusses the recent candidate materials including crystals, semiconductors, and ionically doped glasses. Cooling processes and necessary conditions for cooling are outlined, and general thermodynamic limitations are discussed.

10% wt. Ytterbium doped Yttrium Lithium Fluoride (Yb^{+3}:YLF) is chosen as the candidate active material. The Carnot efficiency for laser and sun-light as a pump source is evaluated using a narrow-band approximation outlined by Stephen and his team. A quantum-mechanical cooling model based on Epstein and his team, is developed. In the proposed system, the candidate material is placed on a magnetically suspended platform inside a vacuum chamber and illuminated with laser light with the appropriate wavelength in the near infrared region. The dynamics of important cooling parameters are simulated and studied. The cooling effects due to radiative relaxation compete with the heating effects due to parasitic absorption and non-radiative relaxation but net cooling is observed confirming validity of light source and material parameter selection.

In addition to laser, the conventional source of pump radiation, sun-light as a pump input to the quantum-mechanical model is simulated and the effects on the cooling power and efficiency are studied. To enhance the energy efficiency of the system, fluorescence recovery schemes using photovoltaics are built and studied. Suggestions for experimental realization are given. The developed model can be base for designing a practical optical refrigeration system for laser and sun-light based optical sources.

ACKNOWLEDGEMENT

I would like to acknowledge the key people who profoundly influenced my work in their own unique style.

Dr. Dirk:

I extend my sincere thanks to Dr. Dirk for accepting and excelling in his role as my thesis supervisor. His expert guidance and support from scope definition, concept refinement to report compilation paved the way for a profound and unique learning experience.

Dr. Peter:

I extend my sincere thanks to Dr. Peter for introducing key concepts in quantum mechanics which were instrumental in model generation. His suggestion for magnetic levitation proved very useful for enhanced thermal isolation of the active material.

Dr. Daniel:

I extend my sincere thanks to Dr. Daniel for helping me understand the foundation behind the "scintillating" phenomenon of optical refrigeration. His creative explanations by drawing parallels between laser and optical refrigerator, elegantly cemented the basics.

Dr. Aurele:

I extend my sincere thanks to Dr. Aurele for providing his expert insights on optics and for introducing the STW valorization grant as a potential financial aid for business realization of the concept.

Family:

I extend my sincere thanks to my brother whose been a constant source for motivation throughout my life. My foray into engineering was inspired by his many ground-breaking inventions. I thank my parents for inculcating within me: love for nature, originality of thought and confidence to follow my heart.

Friends:

I extend my sincere thanks to my friends: Senthil, Austin, Dos, Jeannie, Shruthi, Juan, Andi and Aadi without whom the past three years would not have been remotely as fun.

Table of Contents

GLOSSARY

η_q	Internal quantum efficiency
η_{exe}	External quantum efficiency
η_c	Cooling efficiency
η_{abs}	Absorption efficiency
η_{ext}	Extraction efficiency
η_{PV}	Photovoltaic conversion efficiency
η_{laser}	Laser electrical efficiency
α_b	Parasitic background absorption
α	Resonant absorption
N_t	Population density
N	Number of round trips by the laser beam
σ_{12}	Absorption cross-section
δE_g	Width of ground state manifold
δE_u	Width of excited state manifold
P_{cool}	Cooling power
$P_{laser\ in}$	Incident pump power
$P_{absorbed}$	Absorbed power
$Yb^{3+}:YLF$	Trivalent Ytterbium doped Yttrium Lithium Fluoride crustal
W_r	Radiative recombination rate
W_{nr}	Non-radiative recombination rate

R	Total upper state decay rate
w_g	Thermalization rate for ground state manifold
w_u	Thermalization rate for upper state manifold
ν_f	Mean fluorescence frequency
$\bar{n}$	Average distribution function
$\overline{K}_\omega$	Average radiance
λ_0	Central wavelength
$\Delta\lambda$	Wavelength bandwidth
δ	Beam divergence
T_{F_p}	Flux temperature of pump
T_{F_f}	Flux temperature of fluorescence
T_s	Temperature of the active material
T_c	Temperature of the vacuum chamber walls
ε_c	Emissivity of chamber walls
ε_s	Emissivity of the active material

1. Introduction

Refrigeration is the process of maintaining the temperature of a substance below that of the ambient. Temperature is regarded as a measure of an average kinetic energy of atoms or molecules in a physical system in a state of equilibrium. Thus, refrigeration is associated with reduction of this average kinetic energy. Most common cooling techniques, for example mechanical coolers, are unconcerned with the atomic picture as they operate with macroscopic or ensemble properties of the system. Optical refrigeration or "laser cooling" is best understood in the microscopic pictures, where energy of the system stored in a particular degree of freedom is reduced by the interaction of atoms with light [1].

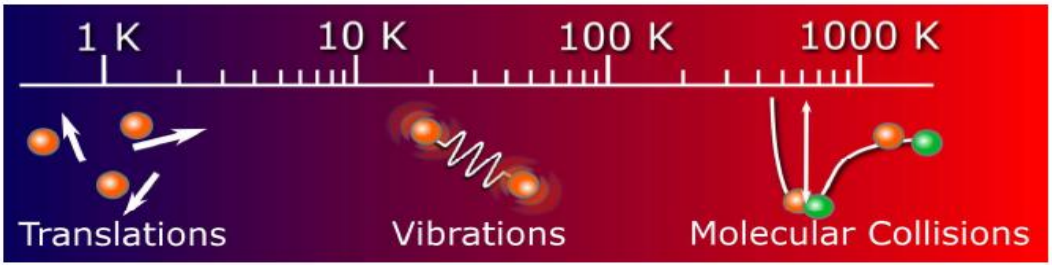

Figure 1 Relevant degrees of freedom, available for laser cooling at various starting temperatures. [1]

From Figure 1, for gases at low temperatures, the thermal energy is primarily contained in translational degree of freedom. In dilute gases at low temperatures, optical refrigeration is realized through Doppler cooling, the demonstration of which was awarded Noble prize in physics in 1997 [2]. When cooled, the kinetic energy of the dilute gas, stored in the translational degree of freedom of the constituents, is reduced via interaction of the Doppler-shifted atomic transitions with counter-propagating laser beams. While Doppler cooling technique works for atoms in diluted gases, it is not suitable for cooling of macroscopic objects like solids where the atomic density is high.

At moderate temperature range of 10 – 400 K (Figure 1), thermal energy of the system is primarily stored in the quanta of the vibrational degrees of freedom, i.e. in the phonons [1]. The vast majority of luminescent materials emit photons with lower energy than absorbed ones [3]. The associated energy difference is the Stokes shift, named after the physicist George G. Stokes. The Stokes shift is based on electron–phonon coupling, which allows pump light to interact with the vibrational modes of solids. This process is accompanied by heat generation in the system. If the emitted photon has more energy than the absorbed one the energy difference between the emitted and absorbed photons is called the anti-Stokes shift and the emitted photons are termed "anti- Stokes fluorescence." This effect is based on dissipation of thermal phonons in a crystal lattice thus resulting in cooling. The idea of optical refrigeration by anti-Stokes fluorescence was first suggested by Pringsheim [4]

Thus, as discussed in the text and with reference to Figure 1 , translations are cooled by Doppler effect, coming into play at very low temperatures and highly diluted gases. Cooling of vibrations through phonon annihilation via anti-Stokes fluorescence is viable in the intermediate temperature range. The latter conditions are typically satisfied in solids and the approach is optical refrigeration of solids [1].

This report focusses on optical refrigeration by anti-stokes fluorescence, as applied to solids.

1.1 Historical development

Denis et al [1] provides a historical overview of optical refrigeration. The idea of optical refrigeration was conceived well before the invention of the laser and was not accepted without controversy. During the 19th century, it was believed that light emitted by a source must always be red-shifted, or equivalently emit at longer wavelengths, as compared to the light absorbed by that source. This was reasoned from the viewpoint of conservation of energy, further verified by experiences that light shining on a material induced heating. The so-called "Stokes' law" stated that: "the rays emitted by a fluorescent substance *always* have a smaller refrangibility than the exciting rays" [5], where the refrangibility, which is related to light's refraction, is equivalent to energy in this context [1].

By the beginning of the 20th century, observations of anti-Stokes radiation refuted the "Stokes' law" and in 1929, Pringsheim suggested the possibility of using the anti-Stokes fluorescence process to cool a fluorescent gas with radiation [4]. This proposal was initially deemed controversial as it was believed to violate the second law of thermodynamics [6]. Pringsheim's ideas were put onto a firm theoretical footing in 1946, when Landau formally assigned entropy to light [7]. The second law states that entropy of an isolated system cannot decrease. Landau pointed out that entropy of the radiation field is a function of both the solid angle of the propagating light and the frequency bandwidth, such that both of these properties have to increase during anti-Stokes fluorescent cooling. In other words, optical cooling is possible when a coherent laser source of low-entropy light with narrow spectral bandwidth and high directionality is converted into a broadband, isotropic luminescence, increasing entropy of the system in the process, even in the presence of local cooling.

1.2 Cooling process

For any object to be cooled, net power output from the system should be larger than the net input power. Thus, for optically cooling a solid, the power of light emitted must be higher than that absorbed. During the process of anti-Stokes fluorescence cooling, incident laser light is converted into isotropic and broadband fluorescence. Since the incident laser light has a small bandwidth and propagates in a well-defined direction, it has almost zero entropy. On the other hand, the fluorescence is broadband and is emitted in all directions; so, if the power of the fluorescence is equal to or greater than the power of the incident beam, the fluorescence has a comparatively large entropy. Therefore, an upper limit on the efficiency of optical cooling will occur when the rate of cooling reduces the entropy of the material being cooled at the same rate at which radiation entropy is generated.

Multiphoton processes are significantly less probable than single-photon emission; so, to achieve a fluorescence (output) power higher than the absorbed power, the substance must emit higher energy photons than it absorbs and do so with a very high (almost unity) quantum efficiency [8]. The general definition of quantum efficiency is the ratio of the number of emitted photons to the number of absorbed photons.

Let's consider a cooling cycle with the active material as trivalent ytterbium ion, a rare-earth material, and the host as glass, an amorphous material. The active material is the one which undergoes the phenomenon of optical refrigeration by anti-stokes fluorescence. Ytterbium in a glass has a number of optical transitions, all centered around a wavelength of ~1µm [8]. Here, optical transitions denote the change in energy level of the trivalent ytterbium ion.

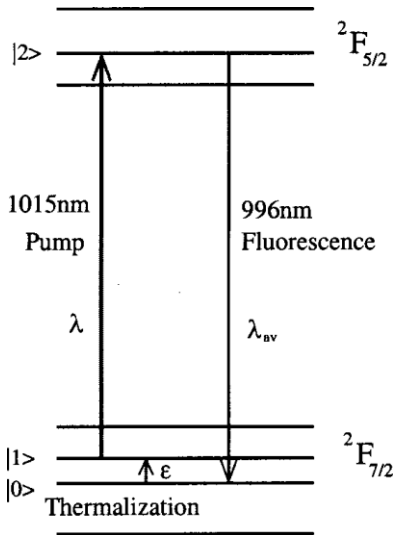

Figure 2 Schematic of optically active energy levels of trivalent ytterbium in a solid host. The solid arrows represent the most strongly allowed optical transitions, which are important for describing the cooling process. The levels involving these transitions are designated for later reference [8]

The simplified level structure for the active material is shown in Figure 1. These levels are shifted by differing amounts depending on the site occupied by the ytterbium atom within the glass, resulting in very broadband absorption and fluorescence spectra. The average emission wavelength at room temperature is 996 nm independent of input wavelength [9]. This is in accordance with Vavilov's empirical rule, which states that the shape of the emission spectrum of a transition is essentially independent of the wavelength at which it is excited [9] Although this is not true for all materials, in the case of ytterbium in glass the time scale of thermal interactions is orders of magnitude shorter (picoseconds to nanoseconds) than the timescale for optical transitions (milliseconds) [10]. This means that, no matter what wavelength is used to excite the ytterbium transition, the population distribution in the upper manifold reaches thermal equilibrium before relaxing to the ground state manifold; so the emission spectrum is independent of pump wavelength, except perhaps at very low temperatures (less than ~ 1 K) [8].

This property can be used to produce a simple model of the cooling process by assuming that this average emission wavelength (996 nm) represents the average behavior of the ytterbium ions. Using this assumption and a pump light (laser input) wavelength of greater than this (say 1015 nm), we arrive at the simplified level structure shown by the arrows in Figure 2.

We can now describe the cooling process that occurs on absorption and emission of a single photon. First an ytterbium ion absorbs an input (pump) photon at wavelength λ; then the ion emits light at wavelength λ_{av} . Finally, the ion absorbs (or releases) thermal energy, or a phonon, from the surrounding glass to return to its initial state.

Assuming the above-mentioned process is 100% efficient and using Planck–Einstein relation we get,

$$\text{Energy lost by glass } = \frac{hc}{\lambda_{av}} - \frac{hc}{\lambda} \tag{1.1}$$

Let the energy of an incident photon be *E*.

$$\text{Energy extracted each time this process occurs } = E\left(\frac{\lambda}{\lambda_{av}} - 1\right) \tag{1.2}$$

Thus, if the pump wavelength is longer than the average, the object will be cooled by this effect, and if the input is a shorter wavelength, heating will occur.

1.3 Conditions for cooling

In reality, the transitions are not 100% optical; one must include the resulting heating [8].

Let Q denote the quantum efficiency of a transition (i.e. radiative relaxation rate/total relaxation rate).

$$\text{Energy extracted per absorbed photon is now } = E\,(Q-1) + EQ\left(\frac{\lambda}{\lambda_{av}} - 1\right) \tag{1.3}$$

Here,

$$E_{heat} = E\,(Q-1)$$
$$E_{cool} = EQ\left(\frac{\lambda}{\lambda_{av}} - 1\right)$$

Thus, the condition for net cooling to result is that $Q\lambda > \lambda_{av}$

Note that this neglects both absorption by the host glass and reabsorption of fluorescence by the ytterbium ions.

We define the coefficient of performance (COP) of the cooling as the difference between the fluorescent energy and the incident energy, normalized by the incident energy. Thus,

$$COP = \frac{Q\left(hf_{fl}\right) - hf_{in}}{hf_{in}} = \frac{Q\left(f_{fl}\right) - f_{in}}{f_{in}} \tag{1.4}$$

Here f_{in} is the frequency of the incident light and f_{fl} is the average emission frequency.

Thus, if the average emission frequency is independent of the incident frequency (as it is in ytterbium-doped ZBLAN or ZBLANP) [8], the cooling power at any input frequency is given by,

$$P_{cool} = P_{in}A(f_{in})\frac{Q\left(f_{fl}\right) - f_{in}}{f_{in}} \tag{1.5}$$

or

$$P_{cool} = P_{in}A(f_{in})\frac{Q\left(\lambda_{in}\right) - \lambda_{fl}}{\lambda_{fl}} \tag{1.6}$$

Here, $A(f_{in})$ represents the absorptivity, P_{in} represents the incident laser power and $\lambda_{fl,in} = {}^{c}/_{f_{fl,in}}$.

2. Candidate solid state active material

For anti-Stokes cooling to be achieved in any solid, a number of conditions need to be met. The high quantum efficiency and low loss of many laser materials make these ideal candidates for anti-Stokes optical cooling. Of these, the best candidates seem to be either semiconductor structures or rare earth ions doped into transparent host materials [8]. The latest breakthroughs in these two types of solid-state active material is covered in this section.

2.1 Rare-earth doped solids

Mansoor Sheik-Bahae et al [11] provides a brief historical development of the candidate active material for optical refrigeration. The advantages of rare-earth (RE) doped solids for laser cooling had been foreseen for decades. Kastler (1950 [12] and Yatsiv (1961 [13] suggested these materials could be used for optical cooling. The key optical transitions in RE ions involve 4f electrons that are shielded by the filled 5s and 6s outer-shells, which limit interactions with the surrounding lattice. Non-radiative decays due to multi-phonon emission are thus suppressed. Hosts with low phonon energy (*e.g.*, fluoride crystals and glasses) further diminish non-radiative decay and hence boost quantum efficiency.

After the invention of the laser in the 1960s, the first attempt to cool a solid was performed by Kushida and Geusic of Bell Telephone Laboratories in 1968 using an Nd3+:YAG crystal [14]. Although the crystal heated, they observed reduced heating as compared with an undoped YAG crystal, leading to the conclusion that heating from impurities was more dominant than the cooling process.

Laser cooling of a solid was first experimentally demonstrated in 1995 with the ytterbium-doped fluorozirconate glass ZBLANP:Yb3+ [10]. In addition to high-quantum efficiency, this host was ideally suited from the material purity requirements benefitting from the developments by the telecommunications industry of low-loss optical fibers in the near-infrared [15].

Markus [16] provides various factors that limit the performance of laser cooling in rare-earth doped active materials. He also discusses the device limitations of potential optical cryo-coolers which won't be discussed here.

2.1.1 Intrinsic material limitations

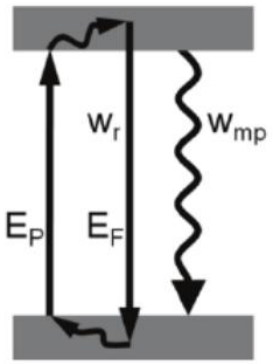

Figure 3 Absorption at energy E_P is followed by thermalization and anti-Stokes fluorescence at energy E_F. Radiative relaxation (straight arrow) and multi-phonon relaxation (wiggly arrow) occur at rates w_r and w_{mp} , respectively. [16]

Optical refrigeration occurs upon absorption of a pump photon of energy E_P, followed by rapid excited-state thermalization and subsequent emission of an anti-Stokes photon at energy E_F. This ideal cooling cycle is illustrated in Figure 3.

The ideal cooling cycle has the following efficiency

$$\eta_{ideal} = \frac{\Delta E}{E_p} \tag{2.1}$$

where, $\Delta E = E_F - E_P$

Alternatively, the excited state can decay non-radiatively via interaction with the optical phonons of the host material (typically the highest-energy optical mode with energy $\hbar\omega_{max}$) and introduce undesired heating through multi-phonon emission.

Internal quantum efficiency signifying the competition between radiative (w_r) and multi-phonon (w_{mp}) relaxation rates is given as

$$\eta = \frac{w_r}{(w_r + w_{mp})} \tag{2.2}$$

Thus, the cooling efficiency is reduced to

$$\eta_{cool} = \frac{(\eta E_F - E_P)}{E_p} \tag{2.3}$$

It is instructive to estimate the parameter space of E_P and $\hbar\omega_{max}$ values that are suited for optical refrigeration. Assuming that a material that realizes $\gamma = 0.9$ of its maximum possible cooling efficiency $\Delta E/E_p$ qualifies as a suited laser-cooling system yields

$$\eta = \frac{(\gamma \Delta E + E_P)}{E_F} \tag{2.4}$$

By substituting internal quantum efficiency and re-arranging the terms, we obtain

$$w_{mp} = \frac{w_r \Delta E(1-\gamma)}{\gamma \Delta E + E_P} \tag{2.5}$$

Firstly, Markus [16] notes that oscillator strengths of 4f-4f transitions of rare-earth ions are $\sim 10^{-6}$ [17], and the corresponding rates for spontaneous radiative relaxation are on the order of $w_r = 100 s^{-1}$. Secondly, he refers to the rate of the multi-phonon energy of the host material given by the energy gap law [18],

$$w_{mp} = \beta \, exp\left(-\alpha E_P / \hbar\omega_{max}\right) \tag{2.6}$$

where $\alpha \; and \; \beta$ are vibrational and electronic parameters of the host material and $\hbar\omega_{max}$ denotes the maximum phonon energy of the host material.

Markus [16] notes that $\Delta E \approx 2.5\, kT$ and finds $\hbar\omega_{max} \approx \left({}^{\alpha E_P}/_{ln\beta}\right)$ at T = 300 K. He referred to a survey of many different materials [19] and found the typical values for α and β on the order of 3.5 and $10^{12}\ s^{-1}$, respectively.
Therefore Markus [16] found that a material can only provide efficient optical refrigeration if

$$\hbar\omega_{max} < {}^{E_P}/_{8} \tag{2.7}$$

Markus [16] constructed a chart (Figure 4) illustrating the above relationship and which can serve as a useful guide in the search of novel candidate material for optical refrigeration.

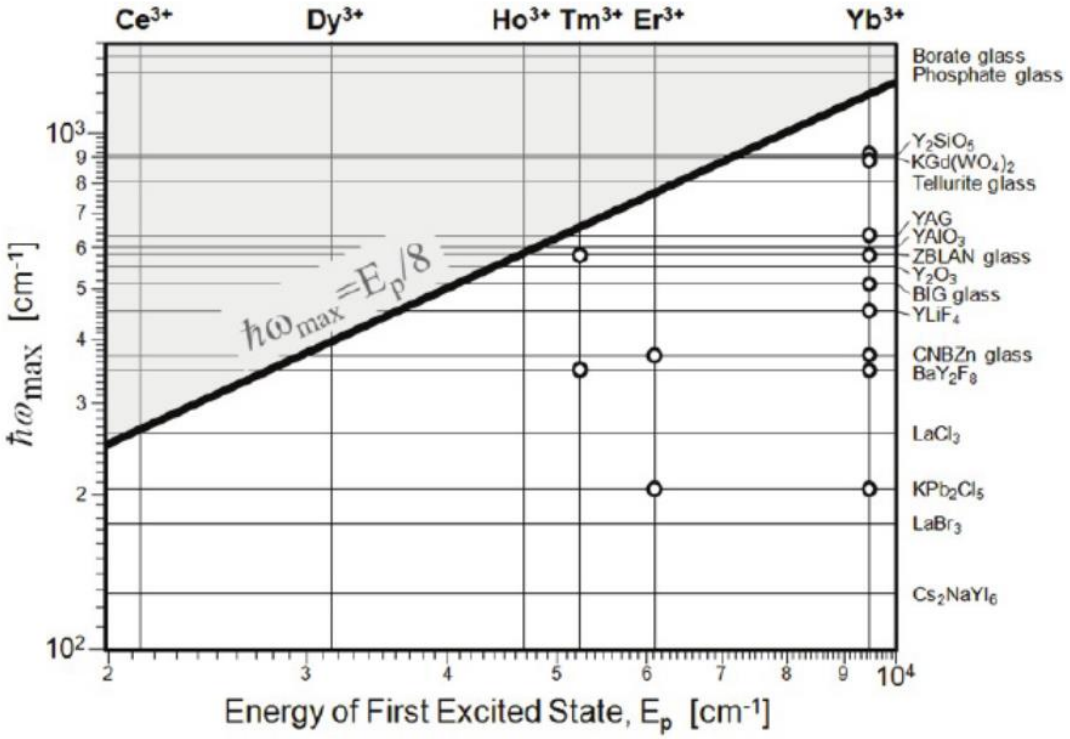

Figure 4 Combinations of active ions and host materials. Systems for which $\hbar\omega_{max} < {}^{E_P}/_{8}$ (below the bold line) have the potential to achieve >90% of their ideal cooling efficiency ${}^{\Delta E}/_{E_p}$. The open circles represent materials for which laser cooling has been experimentally observed until Feb.2009 [16]

Figure 4 shows the maximum phonon energy $\hbar\omega_{max}$ of different glasses and crystals (horizontal lines) and the energy of the first excited *4f* multiplet of different rare-earth ions (vertical lines). Systems below the bold line indicating $\hbar\omega_{max} < {}^{E_P}/_{8}$ have the potential to be efficient optical refrigerators. The circles indicate rare-earth doped solids for which laser cooling has been observed experimentally, confirming the rule of thumb *(2.7)* derived above. The most efficient materials are those with a small E_P , but correspondingly lower $\hbar\omega_{max}$ are required to enable efficient optical refrigeration in such systems.

2.1.2 Material fabrication limitations

Once a suited combination of active ion and host has been identified (Figure 4), the material must be synthesized with both high purity and high optical quality [16].

Impurities can reduce the cooling efficiency in a number of ways [16]:

1. molecules such as OH^- and H_20 can directly coordinate as nearest neighbors to rare-earth ions and quench excited states by multi-phonon relaxation via high-energy vibrational modes;

2. metal ions such as Fe^{2+}, Cu^{2+}, Ni^{2+}, Co^{2+}, V^{3+}, Cr^{3+}, and Ti^{3+} have strong optical absorptions in the visible and near infrared spectral region (up to ~ 2.7μm) and can act as acceptors in non-radiative energy transfers from nearby excited rare-earth ions, followed by multi-phonon relaxation; and

3. the aforementioned metal ions can also directly absorb pump light (background absorption) and subsequently release this energy as heat into the solid by multi-phonon relaxation. Model calculations suggest that the concentration of such impurities must be on the order of 100 parts-per-billion (ppb) or less in order for laser cooling to reach practical efficiencies [20]. Such purities far exceed those of most commercially available precursor materials and, as a consequence, require additional purification during the preparation of the laser-cooling material [16].

Throughout the years, cooling has been observed in a number of materials [1], including:

- **Yb^{3+} doped hosts**: ZBLANP, ZBLAN, ZBLANI, CNBZn, BIG, KGd(WO)4 and KY(WO)4, YAG, Y2SiO5, KPb2Cl5, BaY2F8, YLF, ABCYS;

- **Tm^{3+} doped hosts**: ZBLAN, BYF and YLF;

- **Er^{3+} doped hosts**: CnBZn and KPb2Cl5;

- **Ho^{3+} doped hosts**: YLF;

- **Co-doped hosts**: Co-doping YLF crystals with other upconverting rare-earth ions can enhance cooling through energy transfer enhanced cooling [21]. Recently, co-doped 2% Er^{3+}, 10% Yb^{3+}:YLF nano-particles have shown to refrigerate physiological media [22].

2.1.3 Laser cooling performance comparison of rare earth doped solids

Galina [3] provides an overview on the available candidate material and the net cooling effect observed in them, with trivalent rare-earth as the emitter ion undergoing the anti-stokes fluorescence, in crystalline and amorphous (glass) host. Crystals offer advantages over glass materials such as high thermal conductivity, improved ruggedness, and potentially larger absorption cross sections [23]. Laser cooling performance of top candidates is shown in the following page in Table 1.

Ion	Host		MPE	Nc	Sample (mm)	λ_{pump} (nm)	Pump (W)	T_{start} (K)	Cooling efficiency	Cooling power (mW)	ΔT (K)	Thermal Conductivity (W/mK)	Year
Yb3+	Glass	ZBLAN	580	1 wt%	D = 12, L = 10	1030	1.6	288	1.56%	25	48	0.9	1999 [68]
		ZBLANP	506	2 wt%	D = 8, L = 8	1026	10	300	0.29%	29	92	2 J/K (Sp. heat)	2005 [69]
	Crystal	YAG	630	3 wt%	V = 1 x 1 x 10	1029	4.2	300	1%	8	8.8	13	2013 [75]
		BYF	350	2.50%	V = 3 x 4 x 10	1025	3	293	3%	2.4	4	6	2006 [71]
		YLF	350	10%	V = 4 x 4 x 12	1020	54	265	4%	100	174	~ 4.3 to 6	2015 [67]
Tm3+	Glass	ZBLANP	506	1 wt%	V = 4 x 4 x 8	1900	3.5	~295	3%	na	19	0.17	2003 [23]
	Crystal	BYF	350	1.20%	V = 4.5 x 4.5 x 7	1855	4.4	~295	1%	na	3.2	~ 6.3	2008 [72]
Er3+	Glass	CNBZn	370	0.50%	V = 10.7 x 10.7 x 2.2	860	1.9	301	0.70%	na	0.5	na	2006 [73]
	Crystal	KPC	203	0.50%	V = 4.5 x 6.5 x 2.7	870	1.9	296	0.40%	na	0.7	na	2006 [74]

Table 1 Progress toward net laser cooling in RE doped glasses and crystals with a record temperature drop for each host material. MPE (cm^{-1}), the maximum phonon energy; N_c: the ion concentration; ΔT (K), the temperature drop; λp (nm), the pump wavelength; D(mm), the preform diameter; L(mm), the length of sample; V(mm^3), the volume of the sample, T_{start}, the starting temperature of the sample (K).

2.2 Semiconductor active material

Soon after successful observation of net cooling in Yb-doped glass in 1995 [10], attention was directed towards cooling matter in various condensed phases, beyond rare-earth doped systems. Semiconductors, in particular, have been the focus of numerous theoretical and experimental investigations. The essential difference between semiconductors and RE-doped materials is in their cooling cycles. In the latter, the cooling transition occurs in localized donor ions within the host material while the former involves transition between extended valence and conduction bands of a direct gap semiconductor [1]. The laser cooling of direct-bandgap semiconductors, for example gallium arsenide (GaAs), is more appealing because they allow more efficient pump light absorption, much lower achievable cooling temperatures and direct integrability into electronic and photonic devices [24].

Semiconductors should achieve higher cooling power density compared to RE-materials. The maximum cooling power density (rate of heat removal) is $\approx N \times {}^{k_B T}/_{\tau_r}$ where *N* is the photo-excited electron (-hole) density and τ_r is the radiative recombination time. In semiconductors the optimal density *N* is limited due to many-body processes and does not exceed that of moderately doped RE systems. We can gain 5-6 orders of magnitude in cooling power density because the radiative recombination rates in semiconductors are much faster than in RE ions [11] [25]. Nevertheless, the net cooling of a GaAs based semiconductor has inherent impediments due to high background absorption and low luminescence extraction efficiency, although anti-Stokes up-conversion can be readily achieved [24] [26].

2.2.1 Laser cooling of cadmium sulfide nanobelts

In 2013, a team of Singapore researchers took the scientific community by a surprise by reporting direct laser cooling in CdS nanostructures at $\lambda \sim 520$ nm [27]. These results are extremely interesting since II-VI compounds were not known for having the high quantum efficiency required for laser cooling [1].

According to Sheik-Bahae/Epstein (SBE) theory [11] [28] the cooling efficiency, $\eta_c(h\nu, T)$, of optical refrigeration in semiconductors is given by

$$\eta_c(h\nu, T) = \eta_{exe}\eta_{abs}\frac{\bar{\nu}_f(T)}{\nu} - 1 \tag{2.8}$$

Here ν is the pump laser frequency, T is the absolute temperature of the sample, $\bar{\nu}_f(T)$ is the mean emission frequency and h is Planck's constant.

External quantum efficiency, η_{exe} , describes the efficiency by which a photo-excited atom decays into an escaped fluorescence photon in free space. It is given as follows

$$\eta_{exe} = \frac{\eta_e W_{rad}}{\eta_e W_{rad} + W_{nr}} \tag{2.9}$$

Here η_e is the luminescence extraction efficiency and W_{rad} and W_{nr} are respectively the radiative and non-radiative recombination rates.

Absorption efficiency, η_{abs} , quantifies the percentage of photons absorbed that are engaged in cooling.

Absorption efficiency is given as follows

$$\eta_{abs} = \frac{\alpha(\nu, T)}{\alpha(\nu, T) + \alpha_b} \tag{2.10}$$

Here, α_b is the background absorption coefficient and $\alpha(\nu, T)$ is the semiconductor absorption coefficient. Net laser cooling requires $\eta_c(h\nu, T) > 0$, which can be achieved in three related ways [27]:

1. Having large energy difference $\Delta E = h\bar{\nu}_f(T) - h\nu$
2. Having external quantum efficiency, η_{exe} , approach unity
3. Having absorption efficiency, η_{abs} , approach unity through minimization of α_b

In the classical Pringsheim [4] picture applied to solids, each cooling cycle removes $\Delta E = h\bar{\nu}_f(T) - h\nu \approx k_B T$ during the thermalization of cold electrons and holes, owing to absorption of various phonons. In GaAs, single longitudinal optical phonons (LOP)-assisted transitions in band-tail absorption (Urbach tail) have been proposed to facilitate laser cooling [27] [29] [30]. It has also been proposed that the band structure can be engineered, for example by introducing donor–acceptor pairs, which modifies the density of states and could lead to a larger ΔE, making the dependence on the other two factors (η_{exe} and η_{abs}) less important. However, experimentally that is to achieve because the doping density and binding energies of both donors and acceptors have to be simultaneously optimized [27].

Zhang et al [27] found that strong exciton (bound electron-hole pairs which behave like hydrogen atoms) –LOP coupling in II–VI semiconductors such as cadmium sulphide (CdS) can be exploited to facilitate laser cooling by the annihilation of one or more LOPs, leading to the removal of several $k_B T$ units of heat in each cooling cycle. They demonstrated a substantial net laser cooling of semiconductor CdS nanobelt by $\sim$ 40K from room temperature when pumped by a 514-nm laser, and a net cooling by $\sim$ 15K from 100K when pumped by a 532-nm laser. The belts are stretched across holes in a silicon substrate through which the pump laser is directed. (Reabsorption of the fluorescence is minimal due to the small distance an internally emitted photon has to travel to reach the sample surface.) The nanoribbons of CdS are approximately 100 nm thick, 2 µm wide, and 10 µm long. The exciton-phonon coupling strength is enhanced by the nanoscale size of the ribbons, leading to the annihilation of several LOP per laser photon absorbed and thereby increasing the cooling. The successful cooling is also due in part to the low carrier mobility of CdS which results in a reduced surface recombination rate [27].

Bulk synthesis of cadmium sulfide

In the achievement of net laser cooling in CdS, nanobelt morphology plays an important role in minimizing photon trapping and re-absorption, nonetheless it limits the broader applications due to sample variation and scaling challenges. Therefore, it is important to obtain bulk CdS crystals with similar optical quality towards laser cooling, which shall have important implications in macroscopic optical refrigeration devices. Unfortunately, the trapped state emission (contributed by various kinds of crystalline defects) of commercial or typically synthesized CdS bulk crystals is detrimental for the laser cooling [31]. The trapped state emission would generate heat and diminish the laser cooling performance. The defect accumulation in the process of bulk crystal growth makes it more difficult to obtain ideal upconversion photo luminescence than the nanobelt due to the relative larger size.

Zhang's team [31] have developed the optical floating zone method to synthesize CdS bulk crystals without defect emission at long wavelength, which was attributed to the low synthesis temperature, continuous up-movement of CdS sample rod and fast crystal growth rate. The schematic of the method and crystal morphology is shown in Figure 5.

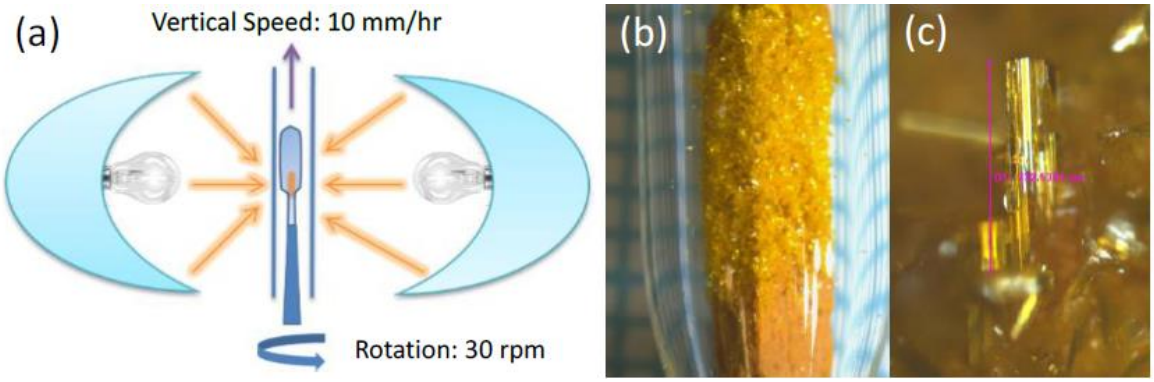

Figure 5 (a) Schematic diagram of optical floating zone for CdS crystals growth; (b), (c) the morphology of the CdS crystals [31]

Zhang's result largely minimized the unwanted heating induced by the long-wavelength emission during the optical process and improve the progress on the laser cooling in CdS bulk crystals. The achievement of net laser cooling in bulk CdS crystal may be still limited by the external quantum efficiency and the absorption efficiency, which have not been investigated for Zhang's samples [31]. The non-radiative recombination and background absorption of materials will generate unwanted parasitic heating preventing the achievement of net cooling. These effects cannot be reflected in the steady-state photoluminescence spectra.

2.2.2 Laser cooling of lead halide pervoskites

In 2015 Zhang's research group demonstrated experimentally that $MAPbI_3$ platelets grown by vapour phase synthesis and $PhEPbI_4$ samples exfoliated from a bulk crystal by solution synthesis can be laser cooled by ~23.0 and 58.7 K, respectively, from room temperature [32]. They based their concept on the recent work which shows that perovskite single crystals possess low trap-state density [33] [34] and high external quantum efficiency [35] , both of which are advantageous for laser cooling if a sufficient photoluminescence (PL) upconversion could be achieved. Interestingly, indeed Zhang et al found that lead halide perovskite crystals in both 3D (*i.e.,* $MAPbI_3$) and 2D (*i.e.,* PhEPbI4) forms shows strong photoluminescence upconversion.

Zhang et al [32] work expands the toolbox for optical refrigeration extensively, considering the numerous combinations of inorganic-organic perovskites. With the facile solution processing and accessible crystallization temperature of those perovskite materials, their work opens up the possibility of laser cooling devices facilely bonded to electronic and optoelectronic thermal load [31]. The remaining challenges are to scale up the current vapor phase or solution synthesis towards a uniform macroscale crystalline film and the proper design of the heat sink, since the thermal conductivity of those perovskites is usually low [32].

2.2.3 Laser cooling performance comparison of semiconductors

The laser cooling performance of available semiconductor candidate active materials is shown below:

Material type	**Active Material**	**Substrate**	**Sample** (in μm)	**Λp** (nm)	**Pump** (mW)	**T_{start}** (K)	**Cooling power** (μW)	**Cooling efficiency**	**ΔT** (K)	**Thermal Conductivity** (W/K)	**Year**
Group II-VI	CdS	Si/SiO2	10 x 2 x 0.1	514	6.3	290	180	1.3 %	40	20	2013 [27]
Group II-VI	CdS	Si/SiO2	10 x 2 x 0.1	532	6.3	290	97	4.8 %[1]	15	20	2013 [27]
Lead halide pervoskite	MAPbI3	muscovite mica	10 x 2	785	0.66	296	8.8	1.84 %	24	0.14	2015 [32]
Lead halide pervoskite	PhEPbI4	silicon	~ 2 mm	565	0.175	296	na	na	58.7	na	2015 [32]

Table 2 Progress of laser cooling of semiconductors. λp is the pump wavelength in nm; ΔT is the temperature drop of the sample; T_{start} is the starting temperature of the sample (K).

From Table 1 and Table 2, the best-in-class laser cooling based temperature reduction is observed in:

- **10% Yb^{3+}: YLF** crystal for rare-earth doped active element and
- **CdS** for semiconductor active element

As seen before, the cooling cycle in semiconductor and rare-earth doped solids is different; cooling transitions occur in localized donor ions within the host in the latter whereas the former involves transition between extended valence and conduction bands. For further modelling and analysis, **10% Yb^{3+}: YLF** is chosen as the candidate active material undergoing bulk optical refrigeration. Although cadmium sulfide has higher cooling power density, it is yet to be scaled up in size, as seen in previous paragraphs. Ytterbium ions are the most common dopant in optical refrigeration and as such, it's properties can be sourced relatively easily upon literature review. For practical implementation in devices, other factors such as thermal conductivity, cost, etc needs to be taken into account.

[1] It is important to note that high cooling efficiency does not necessarily lead to high cooling power as the final cooling power depends on both energy blue shifting parameter and bandtail absorption. Refer supplementary information in article [27] for further information.

3. Cooling potential of optical fields

3.1 General thermodynamic limitation

Ruan et al [2] [36] analyzed the thermodynamics of laser cooling and determined the Carnot efficiency. Consider a control volume that is to be cooled radiatively. In Figure 6, this is labelled "optical refrigerator". The power flow in and out of this control volume reflects the balance of the pump laser, the external thermal load and the fluorescence emission.

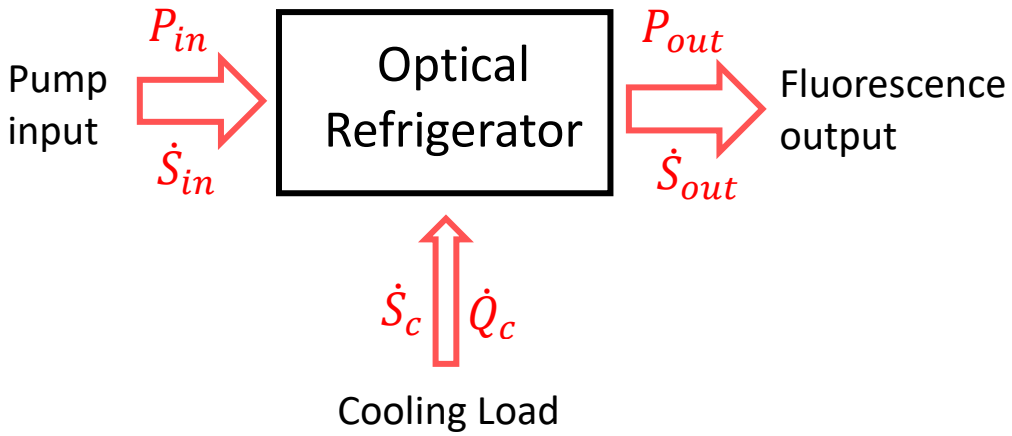

Figure 6 Energy and Entropy flow rates in optical refrigeration process [36]

Applying the 1st law of thermodynamics to the control volume we get

$$P_{out} = P_{in} + \dot{Q}_c \tag{3.1}$$

The cooling efficiency of the process is given by

$$\eta = \frac{\dot{Q}_c}{P_{in}} \tag{3.2}$$

The maximum value of η is the Carnot limit η_c determined by the 2nd law of thermodynamics. The entropy carried by the fluorescence cannot be less than the sum of the entropy withdrawn from the cooling sample and the entropy transported in by the pump laser. That is,

$$\dot{S}_{out} \geq \dot{S}_{in} + \dot{S}_c \tag{3.3}$$

where $\dot{S}_{in}, \dot{S}_{out}$ and $\dot{S}_c$represents the entropy flow rates for the absorbed pump irradiation, output fluorescence and the thermal load.

[2] In the authors analysis, the "dot" over energy terms (thus representing power) is missing

By assuming no irreversibility in the system, eq. (3.3) can also be written as

$$P_{out}\left(\frac{\dot{S}}{P}\right)_{out} = P_{in}\left(\frac{\dot{S}}{P}\right)_{in} + \frac{\dot{Q}_c}{T} \tag{3.4}$$

where T is the temperature of the thermal load.

By substituting Eqs.(3.1) and (3.2) into Eq. (3.4) and by eliminating P_{in}, P_{out} and $\dot{Q}_c$, we find the Carnot efficiency to be

$$\eta_c = \frac{\left[\left(\frac{\dot{S}}{P}\right)_{out} - \left(\frac{\dot{S}}{P}\right)_{in}\right]T}{1 - \left(\frac{\dot{S}}{P}\right)_{out}T} \tag{3.5}$$

Since $\dot{S} = {\dot{Q}}/{T}$ for a reversible process, we can write

$$T_{F_f} = \left({P}/{\dot{S}}\right)_{out} \tag{3.6}$$

$$T_{F_p} = \left({P}/{\dot{S}}\right)_{in} \tag{3.7}$$

Here T_{F_f} and T_{F_p} are called the effective flux temperatures of fluorescence and pump radiation. Substituting Eqs. (3.6) and (3.7) in Eq. (3.5) we obtain the reversible Carnot efficiency as follows

$$\eta_c = \frac{T\left(1 - {T_{F_f}}/{T_{F_p}}\right)}{T_{F_f} - T} \tag{3.8}$$

In the case of near monochromatic and uni-directional pump radiation:

$$\dot{S}_{in} = 0$$

Thus,

$$T_{F_p} \to \infty$$

Landau in 1946 [7] proved for the first time that for monochromatic, unidirectional radiation fluxes, the entropy flux density vanishes.

Substituting the above results in the cooling efficiency, we obtain

$$\eta_c = \frac{T}{T_{F_f} - T} \tag{3.9}$$

From Eq. (3.6) to Eq. (3.9) , the energy, the entropy fluxes and thus the flux temperatures are calculated by treating the radiation fields rigorously as a sum over all radiation modes. It is not possible to do the same analytically for a general input and output field [8]. Rayner et al [8] discussed a simplified analysis from the work of Scovil and co-workers [37] [38] and Weinstein [39] for a general input and output field.

In this approach the pump is assigned in the refrigeration model to the pump laser, the output reservoir being the ideal of a universe at 0 K (coupled through outgoing fluorescence), and the low temperature reservoir being the crystal with coupling through phonon transitions between levels 1 and 2 in Figure 2.

For a general field, the input and output reservoirs are considered to be heat baths with temperatures defined by their respective populations in the upper and lower energy levels. Since the pump laser excites between levels 1 and 2,Figure 2, this definition of an effective temperature can be used to define the effective temperature of pump as

$$T_p = \frac{{}^{E}/_{k_B}}{-\ln({}^{n_2}/_{n_1})}$$

Here E is the transition energy between level 1 and 2, $n_2$and $n_1$are the populations of level 2 and 1, respectively, and k_B is the Boltzmann constant. The temperature of the output reservoir, T_h is defined by an analogous expression involving the levels 2 and 0.

In the example case of laser cooling of solids considered here, the coolant is the Yb^{3+} ions, and the cold reservoir is the ZBLAN host [8]. If this is the case, the above efficiency expression, eq.*(3.9)*, is again obtained, with T_f and T_p replacing the flux temperature equivalents.

Assuming maximum efficiency (i.e., a reversible process), we can simplify the maximum cooling efficiency in Eq.*(3.8)* by substituting for the pump and hot reservoir temperatures in terms of level populations to yield

$$\eta_{c,max} = \frac{\epsilon}{E} \tag{3.10}$$

where ϵ is the energy splitting between levels 0 and 1 and E is the energy of the pump transition from level 1 to 2, Figure 2. This can be understood even more simply by thinking of the process as a cooling cycle, where absorption of energy E causes extraction of energy ϵ.

Since in any real system there will be some losses, the analysis can be extended to incorporate thermal losses that are due to multiphonon transitions between the excited-state and the ground-state manifolds. Rayner et al [8] discusses literary works related to losses occurring in a real system undergoing optical refrigeration. Mungan and Gosnell [40] extend the previous model to incorporate radiative and nonradiative transitions and find that decreasing the transition energy, E, between levels 1 and 2 improves the efficiency even in this case. However, the probability of nonradiative transitions increases

significantly as the transition energy is decreased; so there is some lower limit on the transition energy that can result in efficient cooling. Since the probability of multiphonon transitions also depends strongly on the phonon energies available, this lower limit is highly dependent on the host material. Other possible heating, or thermal loss, mechanisms include absorption by the host material and impurities within it and scattering by the lattice.

3.2 Thermodynamic cooling efficiency for real system including luminescence quantum yield

Ruan et al [3] [36] analyzed the thermodynamics of laser cooling for a real system by including the luminescence quantum yield. In real systems, the luminescence quantum yield is less than unity, and the energy loss during any internal relaxation process is irreversible, from a thermodynamic point of view. When considering such losses caused by nonradiative decay, it is helpful to account for the associated heat load explicitly by dividing the cooling load channel shown earlier in Figure 6 into two parts. In Figure 7 the cooling load channel is now considered to be the reversible part of the refrigerator cycle. No entropy is generated, and the cooling load is still given by Eq. (3.2).

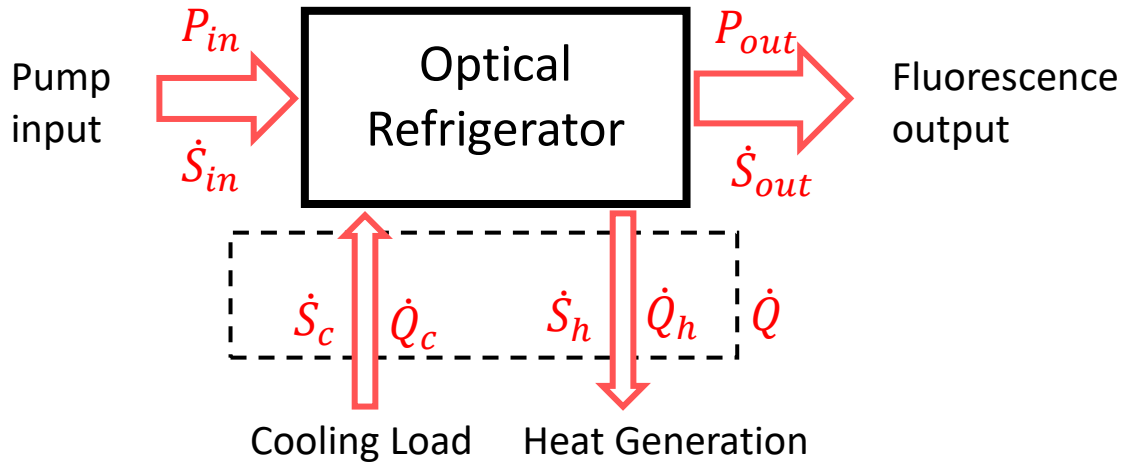

Figure 7 Energy and Entropy flow rates in a real optical refrigeration process [36]

In the figure, the new heat generation channel corresponds to the irreversible losses from internal relaxation.
The entropy production for this channel, also for the entire cooling cycle, is

$$\Delta\dot{S} = \dot{S}_{out} + \dot{S}_h - \dot{S}_{in} - \dot{S}_c = \dot{S}_h - \dot{Q}_h \left(\frac{\dot{S}}{P}\right)_{out}$$

[3] In the authors analysis, the "dot" over energy terms (thus representing power) is missing

$$\Delta\dot{S} = \dot{Q}_h \left[\frac{1}{T} - \left(\frac{\dot{S}}{P}\right)_{out}\right] \tag{3.11}$$

Here, the irreversibility is considered to be introduced when part of the fluorescence output is turned into heat.

The relations between the powers are

$$P_{out} + \dot{Q}_h = P_{in} + \dot{Q}_c \tag{3.12}$$

$$\dot{Q}_c = \eta_c P_{in} \tag{3.13}$$

$$\frac{P_{out}}{P_{out} + \dot{Q}_h} = \eta_q \tag{3.14}$$

where η_q is the luminescence quantum yield.

The net cooling power is then the difference between the cooling load and the heat generation, or

$$\dot{Q} = \dot{Q}_c - \dot{Q}_h = P_{in}\left[\eta_c - (1 + \eta_c)\left(1 - \eta_q\right)\right] \tag{3.15}$$

Cooling coefficient of performance is then

$$COP = \frac{\dot{Q}}{P_{in}} = \eta_c - (1 + \eta_c)\left(1 - \eta_q\right) \tag{3.16}$$

The cooling coefficient has a linear relationship with the luminescence quantum yield. If the luminescence quantum yield is 1, the reversible cycle discussed in the preceding section is recovered, and the cooling coefficient is the Carnot efficiency. In the other extreme, if the luminescence quantum yield is zero, the cooling coefficient becomes −1, indicating that all the laser pumping energy is turned into thermal energy and deposited into the cooling element. There exists a critical luminescence quantum yield $\eta_{q,c}$ below which the cooling effect is eliminated.

3.3 Carnot efficiency for optical fields

3.3.1 Quality of radiation

Stephen. C. Rand et al [41] in their work outlined a new scheme, building on the works of C. Mungan [42] and Landsberg et al [43], to calculate $\frac{\dot{S}}{P}$ of a radiant source by utilizing the central frequency ω_0 and the average distribution function $\bar{n}$ of that source. They tested and established the usefulness of their "narrow-band approximation" to calculate the inverse flux temperature for a wide range of emission fields, seen in Figure 8.

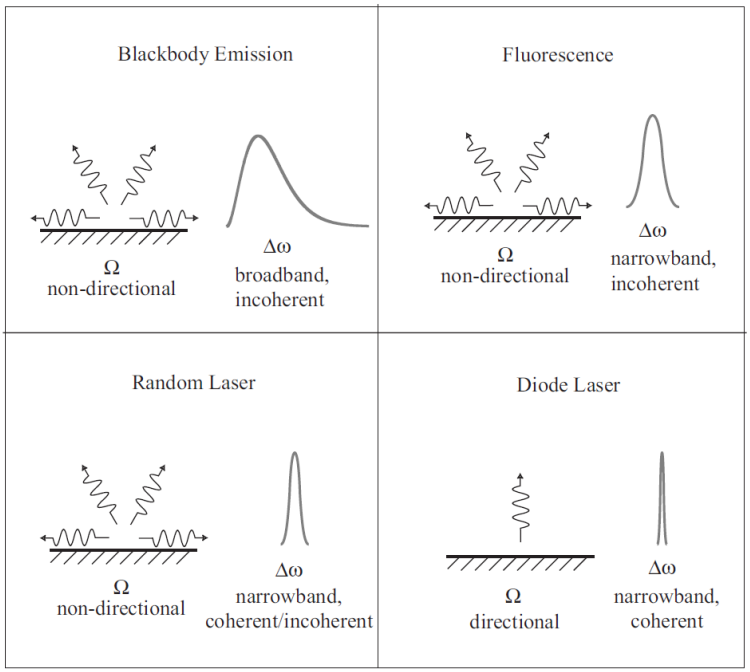

Figure 8 Schematics of emission bandwidth and solid angle associated with the emission fields [41]

From Figure 8, one can observe that

- blackbody sources are spectrally broadband (~ 2223 nm), isotropic in space and incoherent.
- fluorescence sources are spectrally narrowband (~30 nm), isotropic in space and incoherent.
- random lasers are spectrally narrowband (~1 nm), non-directional and can be incoherent.
- diode lasers are spectrally narrow band (~0.1 nm), highly directional and coherent.

Stephen. C. Rand et al [41] concluded that for diode laser as pump (input) field, the most efficient form of radiated (output) field for laser cooling of solids is fluorescence emission, amongst blackbody (4395 K), random laser and diode laser emissions. They based this result on the fact that the inverse of flux temperature, $\frac{\dot{S}}{P}$, was highest for fluorescence amongst the above optical fields. Their analysis is discussed briefly below.

The total power P of a steady, unpolarized beam of light (not necessarily collimated) crossing a surface A, that lies in the x - y plane perpendicular to the direction z of propagation, as given by C. Mungan [42], is

$$P = \iiint_{A\Omega\omega} K_\omega d\omega \ \cos\theta \ d\Omega \ dA \tag{3.17}$$

where K_ω is the spectral radiance, ω is the optical frequency, Ω is the solid angle, and θ is the polar angle between the surface normal and the z axis.

The spectral radiance K_ω, which is the energy per unit time, area, angular frequency, and solid angle, is related to the light source characteristics by

$$K_\omega = \frac{\grave{h} n \omega^3}{4\pi^3 c^2} \tag{3.18}$$

where $\grave{h}$ is the reduced Planck's constant = $\frac{\boldsymbol{h}}{\boldsymbol{2\pi}}$ (for angular frequencies), c is the speed of light in vacuum and n is the photon distribution function which specifies how the radiant energy is distributed among available modes and frequencies.

The entropy of radiation from [43] [42] [41] was shown to be

$$\dot{S} = \iiint_{A\Omega\omega} [(1+n)\ln(1+n) - n\ln n]\omega^2 d\omega \ \cos\theta \ d\Omega \ dA \tag{3.19}$$

Stephen et al [41] introduced a central frequency ω_0 , frequency bandwidth $\Delta\omega$, and divergence angle δ of the beam, to rewrite the beam power Eq. *(3.17*) based on the assumption that the radiation can be treated as "narrow-band". It was shown that if the radiation is narrow-band, and isotropic within the circular cone of half-angle δ , the power of the beam can be approximated to be

$$P = \iiint_{A\Omega\omega} K_\omega d\omega \ \cos\theta \ d\Omega \ dA = \overline{K}_\omega A \ \Delta\omega \ \pi \ \sin^2 \ \delta \tag{3.20}$$

Where $\overline{K}_\omega$ is the mean radiance over the frequency bandwidth and beam solid angle.

From Eq.*(3.18*), an estimated or average distribution function $\bar{n}$ can be defined that is related to the average radiance $\overline{K}_\omega$ through

$$\overline{K}_\omega = \frac{\grave{h} \bar{n} {\omega_0}^3}{4\pi^3 c^2} \tag{3.21}$$

In a similar fashion, entropy flow rate was approximated as

$$\dot{S} = \frac{k_B}{4\pi^3 c^2}\{(1+\bar{n})\ln[(1+\bar{n})] - \bar{n}\ln\bar{n}\}{\omega_0}^2 A\Delta\omega\ \pi\ \sin^2\ \delta \tag{3.22}$$

Thus, dividing Eq.*(3.22)* by*(3.20)*, the entropy flow rate per unit power was shown to be

$$\frac{\dot{S}}{P} = \frac{k_B}{\hbar\omega_0}\left[\frac{(1+\bar{n})\ln[(1+\bar{n})] - \bar{n}\ln\bar{n}}{\bar{n}}\right] \tag{3.23}$$

From Eq.*(3.21)*, $\bar{n}$ is related to average radiance $\bar{K}_\omega$ as follows

$$\bar{n} = \bar{K}_\omega \frac{4\pi^3 c^2}{\hbar{\omega_0}^3} \tag{3.24}$$

By inverting Eq.*(3.20)*, $\bar{K}_\omega$ is found to be

$$\bar{K}_\omega = \frac{P}{A\ \Delta\omega\ \pi\ \sin^2\ \delta} \tag{3.25}$$

Thus, using Eqs. *(3.23)* to *(3.25)* we can determine the Carnot cooling efficiency for the optical fields under investigation.

3.3.2 Carnot efficiency evaluation

From the thermodynamic model detailed in sub-section 3.1, one can observe that pump fields with higher flux temperatures translate to higher Carnot efficiencies. In this sub-section, we will evaluate the inverse of flux temperatures, $\frac{\dot{S}}{P}$, for two distinct input (pump) radiation fields and gauge their corresponding effects on the Carnot cooling efficiency. 10% Yb^{3+}: YLF is chosen as the active material undergoing optical refrigeration. From Table 1, the required pump wavelength is centered around 1020 nm.

The radiant fields under investigation are:

- Laser irradiation
- Solar irradiation

As Solar (black body) radiation is a broad-band emission, we consider an optical filter which receives the radiant field and permits only the required pump wavelengths to irradiate the active material for cooling. The chosen active material is 10% Yb^{3+}: YLF with dimensions: 12 X 4 X 4 (in mm) [44]. Input optical power for solar radiation is 10 mW. This is the power available in the solar radiation (obtained from ASTM standard [45]) for wavelengths between 1010 and 1060 nm. The wavelength range is referred from [46], which provides the necessary input wavelengths in order to observe optical refrigeration in 10% Yb^{3+}: YLF. To form a basis for performance comparison, the optical power of diode laser is chosen to be 10 mW too.

Field 1: Laser irradiation

This is the conventional pumping source employed by scientists researching optical refrigeration; perhaps the reason why optical refrigeration is mostly mentioned as laser cooling in literature. The present report's title explicitly contains optical refrigeration to explore the effects of non-conventional optical source irradiation to achieve cooling via anti-stokes fluorescence. In case1, we evaluate Carnot efficiency for laser irradiation.

Laser parameters:

The laser beam characteristics from literature are tabulated below.

Laser power, P (W)	0.01
Central wavelength, λ_0 (nm)	1020 [47]
Wavelength bandwidth, $\Delta\lambda$ (nm)	0.1331 [41]
Beam diameter, d (μm)	100 [41]
Beam divergence, δ (rad)	0.001 [41]

Table 3 Laser beam parameters [44]

We first evaluate the central frequency $\omega_0 = \frac{2*\pi*c}{\lambda_0} = 1.848 * 10^{15}\ (\frac{\text{rad}}{\text{s}})$

Frequency band-width $\Delta\omega = \frac{2*\pi*c*\Delta\lambda}{{\lambda_0}^2} = 2.411 * 10^{11} (\frac{rad}{s})$

Substituting relevant parameters from Table 3 in Eqs .*(3.25)(3.24*) we obtain the average beam parameters:

Average radiance $\overline{K}_\omega = 1.680 \frac{W}{m^2 \left(\frac{rad}{s}\right) Sr}$

Average distribution function $\bar{n} = 2.818 * 10^7$

Finally, from Eq.*(3.23*) we get,

Entropy flow rate per unit power of laser radiation $\left(\frac{\dot{S}}{P}\right)_{laser} = 4.562 * 10^{-11}\ \text{K}^{-1}$

Fluorescence parameters:

Referring to earlier experiments [44], we find the fluorescence power to be 10.2 mW. This is due to a cooling efficiency of around 2% at 300 K. The fluorescence is assumed to be emitted homogeneously and hemispherically out of the surface of the sample. The fluorescence parameters are tabulated below.

Fluorescence power, P (W)	0.0102
Central wavelength, λ_0 (nm)	999.3 [48]
Wavelength bandwidth, $\Delta\lambda$ (nm)	35 [41]
Beam divergence, δ (rad)	π/2 [41]

Table 4 Fluorescence parameters for laser input

The sample has a dimension of 12 X 4 X 4 mm which leads to a surface area of $2.24 * 10^{-4}$ m^2.

As before, using relevant beam parameters we find

Average radiance $\overline{K}_{\omega} = 2.193 * 10^{-13} \frac{W}{m^2\left(\frac{rad}{s}\right) Sr}$

Average distribution function $\bar{n} = 3.46 * 10^{-6}$

From Eq.*(3.23*) we get,

Entropy flow rate per unit power of fluorescence $\left(\frac{\dot{S}}{P}\right)_{fluorescence} = 9.421 * 10^{-4}\ \mathrm{K}^{-1}$

Now that we have entropy flow rate per unit power of both input and output fields, we can evaluate the Carnot cooling efficiency outlined in the previous section for different sample temperatures.

Field 2: Solar irradiation

Here we assume the presence of a filter, encapsulating the sample, which permits only the required wavelengths to result in cooling of the active material and reflects the rest. We consider the same input power, active material and dimensions as of the previous case of laser input.

Stephen. C. Rand et al [41] reported excellent agreement of their narrow-band approximation with the exact approach of entropy flow rate by power values, for a wide range of blackbody temperatures.

Black body emission power is

$$P = \sigma_{SB} * A * T_b^4 \tag{3.26}$$

Here σ_{SB} is the Stefan-Boltzmann constant and T_b is the temperature of the cavity which emits black-body radiation.

The corresponding entropy flow rate [41] is

$$\dot{S} = \frac{4}{3} * \sigma_{SB} * A * T_b^4 \tag{3.27}$$

Dividing Eq. *(3.27*) by *(3.26*) the entropy flow rate by power is

$$\frac{\dot{S}}{P} = \frac{4}{3T_b} \tag{3.28}$$

Considering Sun's surface temperature to be approximately 5800 K [49], we find the entropy flow rate by power of solar radiation to be $= 2.2988 * 10^{-4}\ K^{-1}$.

Fluorescence parameters:

Fluorescence parameters is same as of previous laser input case (same cooling efficiency & input power).

Thus, entropy flow rate per unit power of fluorescence $\left(\frac{\dot{S}}{P}\right)_{fluorescence} = 9.421 * 10^{-4}\ \mathrm{K}^{-1}$

Carnot efficiency for the optical fields

The input and output entropy flow rates of the two optical fields are substituted in the Carnot cooling efficiency equation discussed in the previous section and a graph is plotted using MATLAB.

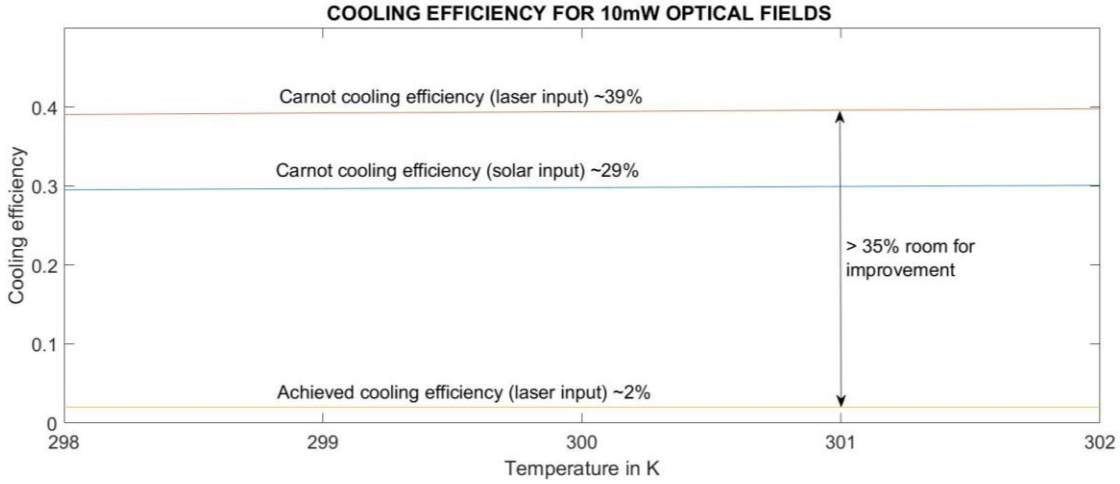

Figure 9 Carnot cooling efficiency

From Figure 9, one can observe that while the present cooling efficiency of optical refrigeration via laser input is only 2% at room temperature [44], the limiting efficiency can be as high as ~ 39%. Hence, there must be a significant amount of irreversibility present in the experiments. For instance, non-radiative relaxation and absorption of the laser by impurities reduce practical cooling efficiencies. For an ion-host combination wherein there is reduced transition energy gap between ground and excited energy states, the cooling efficiency theoretically is higher. However, for long wavelength (reduced energy) pumping, the absorption by trace impurities might suppress the cooling effect produced by the emitter [41]. Furthermore, for this strategy of enhancing cooling efficiency to work, the emitter must have high absorption co-efficient at such longer wavelengths. The material parameters and their role in optical refrigeration will be explained in the following section which contains a quantum-mechanical model of this cooling process.

For the solar pumping case, the Carnot cooling efficiency is surprisingly only 10% lower than the Carnot efficiency for laser irradiation, and the efficiency value is ~ 29%. This is the case for solar radiation uniformly illuminating the active material geometry, with input power of 10 mW. This power value was found referring to ASTM G-173 [45] standard containing the spectral distribution of solar radiation (only direct and circumsolar radiation components was considered) and selecting the appropriate wavelengths at 300 K sample temperature to observe cooling [44]. By choosing appropriate mechanisms/strategies to reduce the entropy flow rate of input solar radiation, e.g. by having concentrators to enhance radiance, this efficiency will climb further. Further modifications for enhancing the cooling performance under solar irradiation is detailed in the following sections.

4. 4-level model for optical refrigeration

4.1 Theoretical framework

Sheik Bahae and Richard Epstein [50] developed a 4-level model in 2008 for solid-state optical refrigeration. Despite its simplicity, this model reveals essential features of the cooling process. The present report utilizes the 4-level model in its theoretical framework.

The cooling cycle for a typical rare-earth ion involves transition between ground state and excited manifolds containing multiple levels. As a consequence of crystal field created by the electric charges of neighboring ions in the solid host, the (2J+1)-fold degeneracy of each manifold is partially lifted via the Stark effect, leading to (2J+1)/2 levels where J is the total angular momentum [47]. Considering Yb^{3+} ions doped in YLF, the crystal field splits the $^2F_{7/2}$ ground state and $^2F_{5/2}$ excited states into manifolds containing 4 and 3 levels respectively as shown in Figure 10a .

To elucidate the essential roles that the various material parameters play in the process of optical refrigeration, it is highly instructive to introduce a simplified 4-level model that will be generally applicable to any such two-manifold cooling system [47].

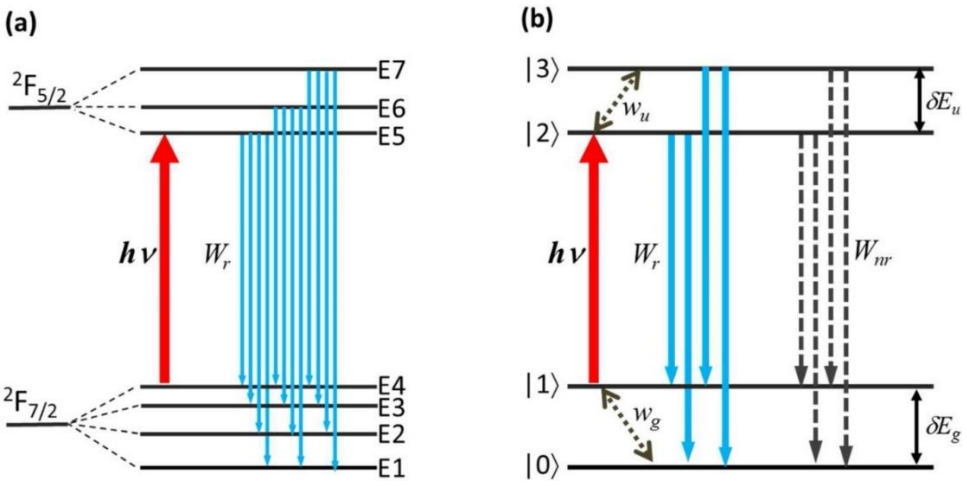

Figure 10 Energy level structure of Yb3+, after partially lifted degeneracy in 7 levels forming ground state (E1-E4) and excited state (E5-E7) state manifolds. (b) Simplified four-level mode for optical refrigeration consisting of two pairs of closely spaced levels: |0> and |1> in the ground state and |2> and |3> in the excited state manifolds [47]

As shown in Figure 10b, this model involves a two-level ground state having a separation that represents the width of the ground-state manifold δE_g, and similarly, a two-level excited state having an energy splitting corresponding to the width of the excited state manifold δE_u. The laser excitation is assumed to take place between levels 1 and 2 ($h\nu = E_2 - E_1$). The electron–phonon interaction, albeit weak for the 4f electrons in the rare-earth ions, establishes Boltzmann quasi-equilibrium within each two-level manifold on a relatively fast (picoseconds to nanoseconds) timescale with corresponding rates given by w_g and w_u. The excitation then decays into ground state by radiative (solid downward arrows) and nonradiative (dotted downward arrows) relaxations with the corresponding rates of W_r and W_{nr} which are much smaller than the thermalization rates $w_{g,u}$.

Following these assumptions, we construct a set of rate equations governing the density populations N_0, N_1, N_2 and N_3:

$$\frac{\mathrm{dN}_1}{\mathrm{dt}} = -\sigma_{12}\left(\mathrm{N}_1 - \frac{g_1}{g_2}\mathrm{N}_2\right)\frac{I}{h\nu} + \frac{R}{2}(\mathrm{N}_2 + \mathrm{N}_3) - w_g\left(\mathrm{N}_1 - \frac{g_1}{g_0}\mathrm{N}_0 e^{-\delta E_g/k_B T}\right) \tag{4.1}$$

$$\frac{\mathrm{dN}_2}{\mathrm{dt}} = \sigma_{12}\left(\mathrm{N}_1 - \frac{g_1}{g_2}\mathrm{N}_2\right)\frac{I}{h\nu} - R\mathrm{N}_2 + w_u\left(\mathrm{N}_3 - \frac{g_3}{g_2}\mathrm{N}_2 e^{-\delta E_u/k_B T}\right) \tag{4.2}$$

$$\frac{\mathrm{dN}_3}{\mathrm{dt}} = R\mathrm{N}_3 - w_2\left(\mathrm{N}_3 - \frac{g_3}{g_2}\mathrm{N}_2 e^{-\delta E_u/k_B T}\right) \tag{4.3}$$

$$\mathrm{N} = \mathrm{N}_0 + \mathrm{N}_1 + \mathrm{N}_2 + \mathrm{N}_3 \tag{4.4}$$

where $R = 2W_r + 2W_{nr}$ is the total upper state decay rate, σ_{12} is the absorption cross section associated with $|1\rangle$ - $|2\rangle$ transition, I is the incident laser irradiance and the g_i terms represent degeneracy factors for each level. The weighting factor in the electron–phonon interaction terms (w_u and w_g) maintains the Boltzmann distribution among each manifold at quasi equilibrium.

The net power density deposited in the system is the difference between the absorbed and the radiated contributions:

$$\mathrm{P}_{net} = \sigma_{12}\left(\mathrm{N}_1 - \frac{g_1\mathrm{N}_2}{g_2\mathrm{N}_1}\right)I - W_r[\mathrm{N}_2(E_{21} + E_{20}) + \mathrm{N}_3(E_{31} + E_{30})] + \alpha_b I \tag{4.5}$$

Here the first term is the laser excitation ($|1\rangle$-$|2\rangle$ transition) and second term includes the spontaneous (i.e. fluorescence) emission terms from levels $|2\rangle$ and $|3\rangle$ with their respective photon energies. The last term represents "parasitic absorption" of the pump laser with an absorption coefficient of α_b.

It is straightforward to evaluate the steady-state solution to the above rate equations by setting the time derivatives to zero. For simplicity, we further assume equal degeneracy for all four levels thus eliminating the *g*-ratio terms [50]. The set of equations Eq.*(4.1)* -*(4.3)* can be solved to obtain the steady-state population in each level in terms of laser intensity and the given material parameters. The absorption of the pump laser and its saturation behavior (assuming homogenously-broadened vibronic levels) is given as follows [47]:

$$\alpha = \frac{\alpha_0}{1 + \frac{I}{I_s}} \tag{4.6}$$

where

$$\alpha_0 = \sigma_{12}\mathrm{N}_t \frac{e^{-\delta E_g/k_B T}}{1 + e^{-\delta E_g/k_B T}} \tag{4.7}$$

and

$$I_s = \frac{h\nu_{12}R}{\sigma_{12}Z_{gu}} \tag{4.8}$$

with $Z_{gu} \approx 1 + e^{-\delta E_g / k_B T}$ [47].

The net power density is then obtained as:

$$\mathrm{P}_{net} = \alpha I\left(1 - \eta_q \frac{h\nu_f}{h\nu}\right) + \alpha_b I \tag{4.9}$$

where $\eta_q = \frac{W_r}{W_r + W_{nr}}$ is the internal quantum efficiency. For semiconductor active materials where refractive index is large enough for re-absorption of the fluorescence, external quantum efficiency η_{ext} is used: $\eta_{ext} = \frac{\eta_e W_r}{\eta_e W + W_{nr}}$. Here η_e represents the extraction efficiency which is the fraction of the emitted photons leaving the sample. Rare-earth doped solids typically have very high extraction efficiency [47] due to low index of refraction thus external quantum efficiency is equal to η_q.

The mean fluorescence energy $h\nu_f$ is given by [50]:

$$h\nu_f = h\nu + \frac{\delta E_g}{2} + \frac{\delta E_u}{1 + \left(1 + R/w_u\right) e^{\delta E_u / k_B T}} \tag{4.10}$$

Dividing Eq.*(4.9)* by the total absorbed power density $P_{abs} = (\alpha + \alpha_b)I$ gives the cooling efficiency

$$\eta_c = \eta_q \eta_{abs} \frac{h\nu_f}{h\nu} - 1 \tag{4.11}$$

where $\eta_{abs} = \frac{\alpha}{\alpha + \alpha_b}$ is the absorption efficiency.

The most useful feature of the 4-level model is its description of the temperature-dependence of the cooling in a physically transparent manner:

- From Eq.*(4.7)* pump absorption reduces due to thermal depletion of the top ground state at low temperatures, $k_B T < \delta E_g$. This implies the width of the ground-state manifold (δE_g) must be narrow to achieve low temperatures with reasonable efficiency, e.g. fluoride host materials [47].
- From Eq.*(4.10)* the mean fluorescence photon energy is red shifted (wavelength increases) at low temperatures, which further lowers the cooling efficiency.
- From Eq.*(4.11)* the lowest temperature $T = T_m$ will be achieved when $\eta_c(T_m) \to 0$. The minimum temperature achieved to date is 91K [44].

4.1.1 Yb^{3+} energy level

Bensalah et al [51] made detailed analysis of Yb^{3+}-doped YLF spectroscopy for the determination of energy levels of the Stark splitting in this host. Their result is shown in Figure 11.

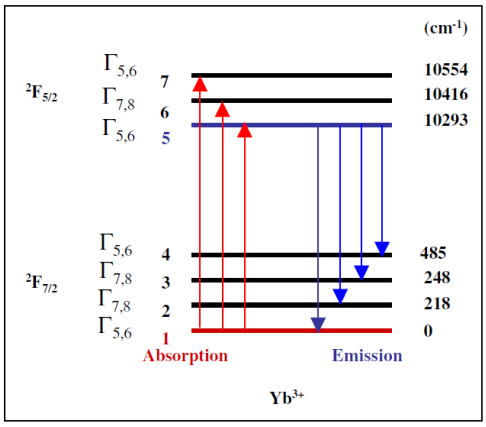

Figure 11 Energy levels of Yb^{3+} in YLF [51]

Wavenumber is provided for each energy levels in the Figure 11. Wavenumber (in cm^{-1}) is simply the inverse of wavelength. Thus, wavenumber can be used to calculate the energy difference between levels.

4.1.2 Ground state absorption

Anti-Stokes fluorescence relies on the absorption of photons red-shifted from the mean luminescence wavelength. Calculating the absorption by measuring the emission is done using a reciprocal relationship between the absorption and emission cross-sections that was first established by McCumber [52].

The absorption cross-section is given as follows [53]:

$$\sigma_{12}(\nu) = \sigma_{21}(\nu)\,\frac{Z_l}{Z_u}\,exp\left[{(E_{ZL} - h\nu)}/{k_B T}\right] \tag{4.12}$$

Where Z_l and Z_u are the partition function in the lower and upper manifold given by

$$Z_k = \sum_k d_k\, exp\left[{-E_k}/{k_B T}\right] \tag{4.13}$$

Here k = l , u (lower, upper manifold)

By assuming equal degeneracy in each manifold, the ratio of partition function term then carries no degeneracy. The term E_{ZL} is the zero-line energy given by the energy separation between the lowest components of the upper and lower manifolds.

A. Bensalah et al [51] performed detailed spectroscopic analysis and obtained, for both π (parallel) and σ (transverse) polarizations, the infrared (IR) emission spectra:

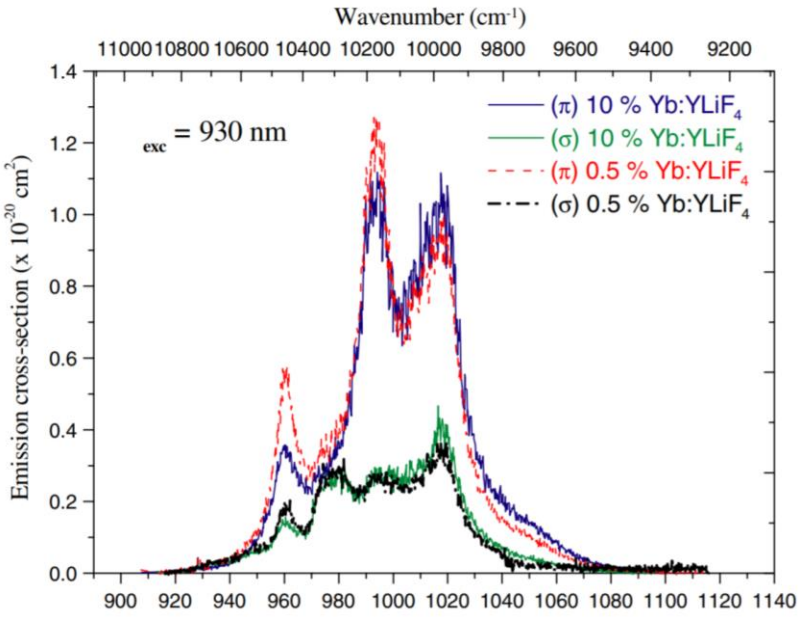

Figure 12 Polarized emission cross-section of 10% and 0.5% Yb^{3+}-doped YLiF4 [51]

From the previous figure, for a particular frequency, the emission cross-sections for both π and σ polarization can be found. These two values can be averaged [54] to obtain the final emission cross-section $\sigma_{21}(\nu)$. Then using Eq.*(4.12)* the absorption cross-section $\sigma_{12}(\nu)$ can be found for that frequency and at the temperature of interest. Some researchers geometrically modified the active material to utilize a polarized light input and obtained enhanced absorption cross-section [44]. Assuming similar geometric modification, from Figure 12, we find $\sigma_{12}(\nu)$ assuming π polarized absorption. Then, ground state absorption coefficient, α, is calculated from Eq.*(4.6)*.

4.1.3 Other material parameters

The other material parameters required for determining the cooling power and thus the cooling efficiency are referred from a variety of sources and are tabulated in Table 5.

Emitter: 10 mol% Yb^{3+}, Host: YLF. Active material dimensions: l = 12mm, b = 4 mm & h = 4 mm

Material parameter	value	Reference
Thermalization rates for upper and lower manifolds, w_u, w_g	$\sim 10^{12} s^{-1}$	[55]
Radiative relaxation rate, W_r	$314.46\ s^{-1}$	[51]
Quantum efficiency, η_q	*0.995*	[56]
Background absorption, α_b	$2.603 * 10^{-8}\ eV$	[57]
Number of Yb^{3+} ions per unit volume, N_t	$1.4 * 10^{27}\ m^3$	[58]
Width of ground state manifold, δE_g	*0.06013 eV*	Figure 11
Width of upper state manifold, δE_u	*0.03236 eV*	Figure 11

Table 5 Material parameters for 10% doped YB3+ YLF

4.2 Laser input to 4-level model

4.2.1 Cooling setup

The cooling setup is shown below. Chamber dimensions: l = 13 mm, b = 5 mm & h = 5 mm
Essentially the chamber dimensions are chosen to be sample dimension + 1mm to reduced radiative heat load as will be discussed in the bulk cooling section later.

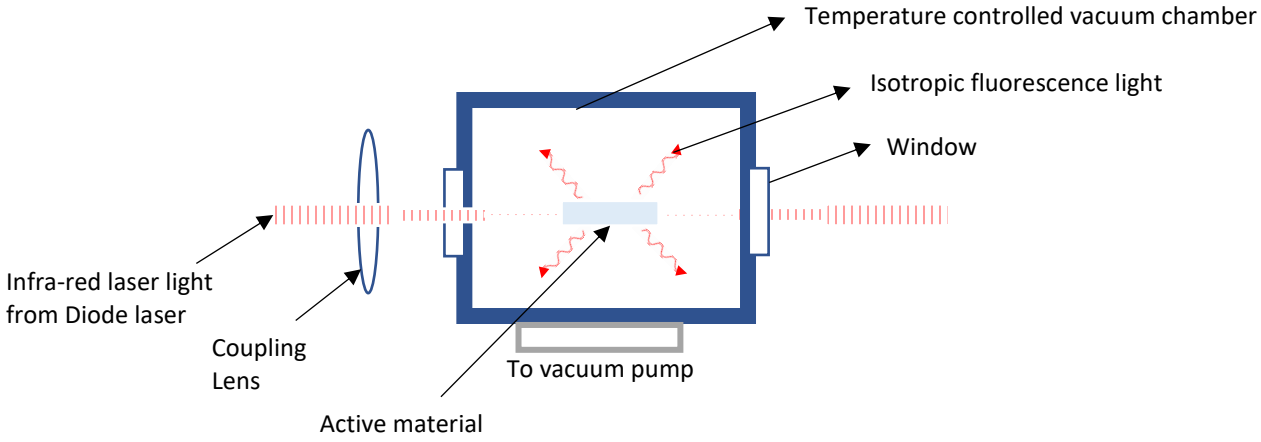

Figure 13 Top view of the cooling setup. For better fluorescence representation the figure is not drawn to scale.

4.2.2 Pump characteristics

- Continuous wave NIR (near infra-red) laser
- Optical power of the laser beam [44] = 54 W
- Beam diameter = 500 µm
- Wavelength of the beam = 1020 nm

4.2.3 Bulk cooling

The performance of a solid-state optical refrigerator is determined by the competition between the cooling power, P_{cool}, and the heat load on the cooling element, P_{load}. The change in temperature of the cooling element is given by:

$$C(T)\frac{dT}{dt} = -P_{cool} + P_{load} \tag{4.14}$$

Where $C(T) = c_v(T) * \rho * V_s$ is the heat capacity, which depends on the specific heat, $c_v(T)$, the density, ρ, and the sample volume, V_s. Density is taken as $4.07 * 10^6 \frac{g}{m^3}$ [59]. The Debye model provides a good description of the temperature dependence of the specific heat of dielectric crystals [59]. In this model, the specific heat at constant volume is given by:

$$c_v = \left(\frac{9nN_A k_B}{M}\right)\left(\frac{T}{\theta_D}\right)^3 \int_0^{x_m} \frac{x^4 e^x}{(e^x - 1)^2} dx \quad (4.15)$$

where c_v is the specific heat at constant volume, n is the total number of atoms in the chemical formula (6), N_A is the Avogadro constant, k_B is the Boltzmann constant, M is the molecular weight (172.09 g/mol), $x_m = {\theta_D}/{T}$ and θ_D is the Debye Temperature (560 K).

In thermal equilibrium, $\frac{dT}{dt} = 0$, $P_{cool} = P_{load}$. The heat load power has contributions from convective, conductive and radiative heat transfer from the environment to the cooling element, $P_{load} = P_{convective} + P_{conductive} + P_{radiative}$.The first two respective heat load contributions are lowered by carrying out the experiment in a vacuum chamber, by minimizing the contract area between the sample and its supports and choosing supports with low thermal conductivity. Detailed modeling has shown that under these conditions the radiative or blackbody load is indeed the dominant contribution [60] [61] [62]. It was shown that the radiative load ($\sim 2.4 * 10^{-4} \frac{W}{k}$) dominates the convective and conductive contributions by factors of $1.2 * 10^3$ and $2.0 * 10^1$, respectively.

An embodiment for minimized conductive heat load can also be achieved by magnetically levitating a platform which supports the active material. Thus, in this case the sample no-longer has any mechanical contact with the "hot" chamber walls and the conductive heat load contribution is further reduced. Care should be taken that the levitating platform doesn't absorb the high energy fluorescence emanating from the cooling crystal. If this happens, the conductive heat load will increase as the platform heats up. It's also necessary that the fluorescence doesn't reflect off this platform and irradiate the sample, as then it would lead to direct sample heating. Thus, for any thermal management application of an optical refrigerator, care should be taken to dispose off the fluorescence light by proper "light" management. In some embodiments of optical refrigerator, a separate cooling link is designed which has contact with the active material and an external cooling load in such a fashion that it provides a good thermal pathway but not an optical pathway to the cooling load [47]. Thus, such cooling links must have high thermal conductivity and very low absorptivity for both fluorescence and (scattered) pump light. In this report, only the dominant heat load contribution, radiative heat load from the surrounding chamber, is considered. The radiative heat load can then be approximated [54] [60] [56] [47] as

$$P_{radiative} = \frac{\varepsilon_s A_s \sigma}{1 + \chi}(T_c^4 - T_s^4) \quad (4.16)$$

Where $\chi = (1 - \varepsilon_c)\varepsilon_s A_s / \varepsilon_c A_c)$ is an experimental pre-factor, the Stefan-Boltzmann constant is $\sigma = 5.67 * 10^{-8}\ w/m^2/K^4$, ε are the thermal emissivities of the laser-cooling crystal (s) and the clamshell (c), and A are the surface areas of the laser-cooling crystal (s) and the clamshell (c). To maximize χ (for minimization of $P_{radiative}$), the vacuum chamber dimensions are chosen to be close to the sample dimension such that $A_s/A_c \approx 1$. Furthermore, the vacuum chamber has a very low emissivity ε_c in order to maximize χ. Acktar MAXi BLACK[4] polymer film is chosen to line the inner walls of the vacuum chamber. This special coating has an incredibly low emissivity $\varepsilon_c = 0.01$. The emissivity of the sample is $\varepsilon_s = 0.8$ [46].

[4] http://www.acktar.com/product/maxiblack/?_sfm_product_technology=optical-systems&_sfm_product_wave_length=NIR

The negative contribution on the right-hand side of Eq. *(4.14*) is given by Beer-Lamberts law [47]:

$$P_{cool} = \eta_c(\lambda, T) * P_{laser\ in}(1 - e^{-N*\alpha(\lambda,T)*L}) \tag{4.17}$$

a product of the cooling efficiency and the absorbed power ($P_{absorbed}$) which in turn is given as a product of the laser input power ($P_{laser\ in}$) and the absorbance term in the brackets, which depends on the resonant absorption coefficient $\alpha(\lambda, T)$ and an effective interaction length $N * L$. Thus, by enhancing the number of round trips N and absorption coefficient α, we can enhance the cooling power.

4.2.4 Cooling results for laser irradiation

1) Temperature vs Time

The below graph is the result of a simulation run with MATLAB, with the aforementioned material parameters, with the chamber wall maintained at constant 300 K, a single pass of the pump beam and with a 1 second time step. We observe an initial rapid pull-down of temperature, ΔT = 100 in ~ 3 minutes, and from then onwards the temperature decline slows down. The final temperature at the end of 12 minutes is 124 K. To better understand the temporal evolution of the graph, we look at the dynamics of other performance parameters.

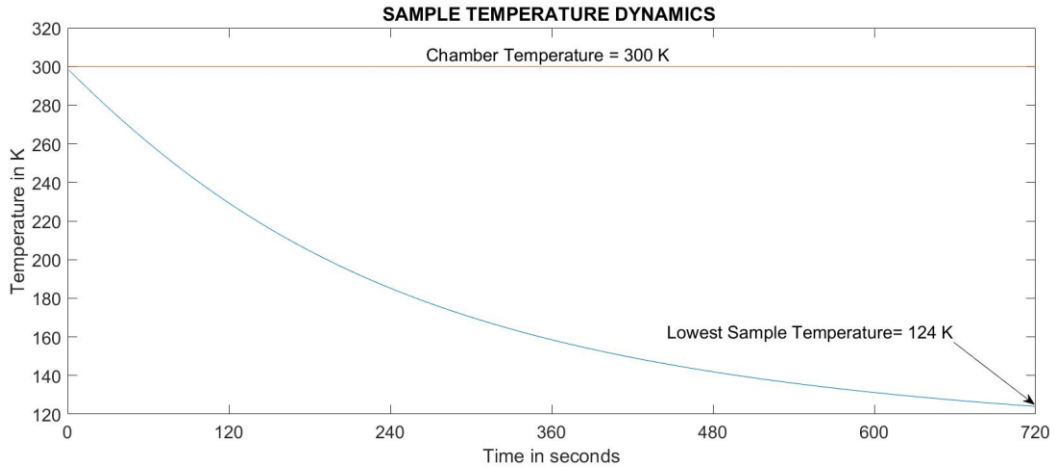

Figure 14 Temperature pull-down simulation by 4-level optical refrigeration model

2) Cooling Efficiency vs Time

The cooling efficiency dynamics is shown in the following page. At initial sample temperature, the cooling efficiency is around 1.9%. As the temperature of the active material reduces, the cooling efficiency lowers. This reduction in the cooling efficiency can be attributed to: (i) the reduced absorption of the ytterbium ions at lower temperature and (ii) red-shifting of the mean fluorescence wavelength at lower temperatures. It's interesting to observe that cooling efficiency doesn't vanish completely; cooling still happens but the temperature of the sample almost equilibrates to 124 K from the previous graph. Thus, if pump absorption is enhanced, further temperature reduction is imminent.

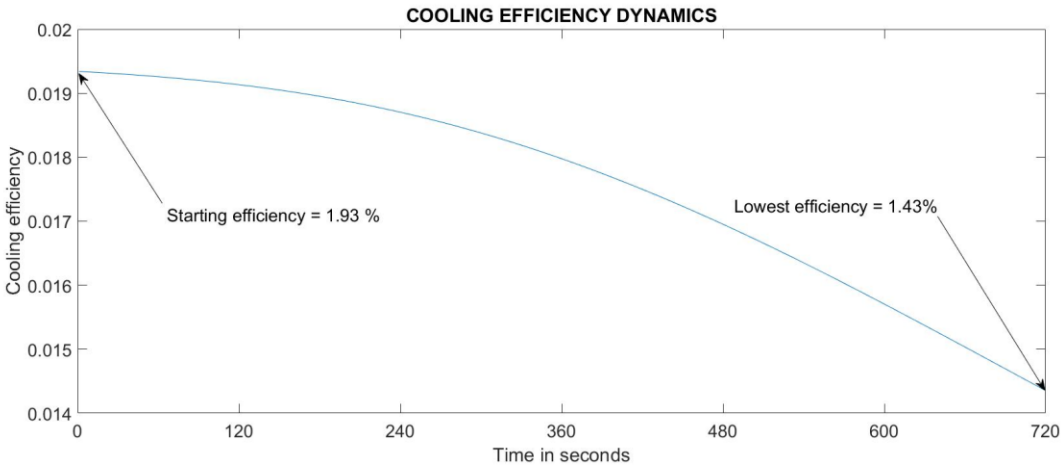

Figure 15 Cooling efficiency dynamics by 4-level optical refrigeration model

3) Cooling Power vs Time

From the below graph, we obtain a cooling power of 400 mW at 298.15 K. As time progresses and the temperature reduces, the cooling power reduces due to reduced absorption coefficient and reduced cooling efficiency at lower temperatures. The heat lift at 124 K is found to be 17.8 mW. Cooling power can be enhanced by enhancing the number of pump beam passes.

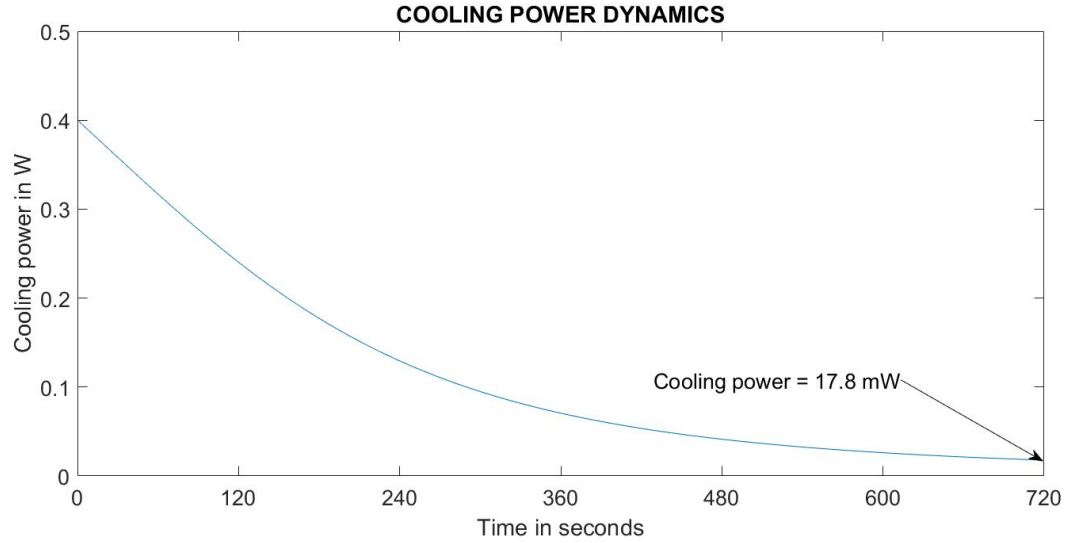

Figure 16 Cooling power dynamics by 4-level optical refrigeration model

4) Fraction of pump power absorbed vs Time

Figure 17 in the following page clearly indicates the need for having more pump beam passes. Without a multi-pass scheme, a maximum of only 39% incident laser light is absorbed by the ytterbium ions. Thus, by enhancing the absorption power by having a multi-pass scheme, it is possible to reach temperatures lower than the one in Figure 14.

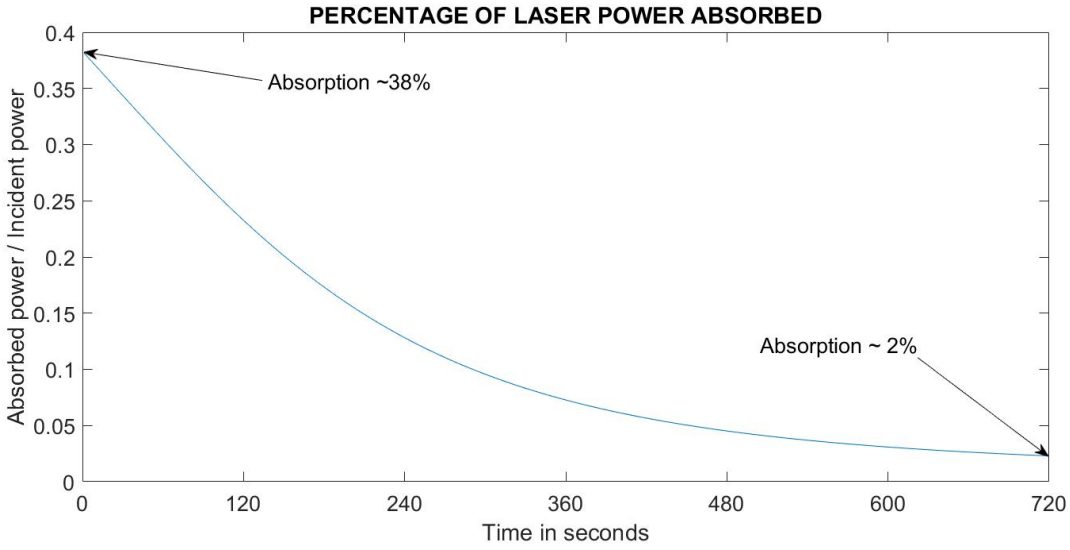

Figure 17 Dynamics of percentage of pump light absorption by 4-level optical refrigeration model

A multi-pass scheme with 1, 5 and 10 beam passes is simulated with MATLAB and the temperature dynamics of the system are plotted in Figure 18.

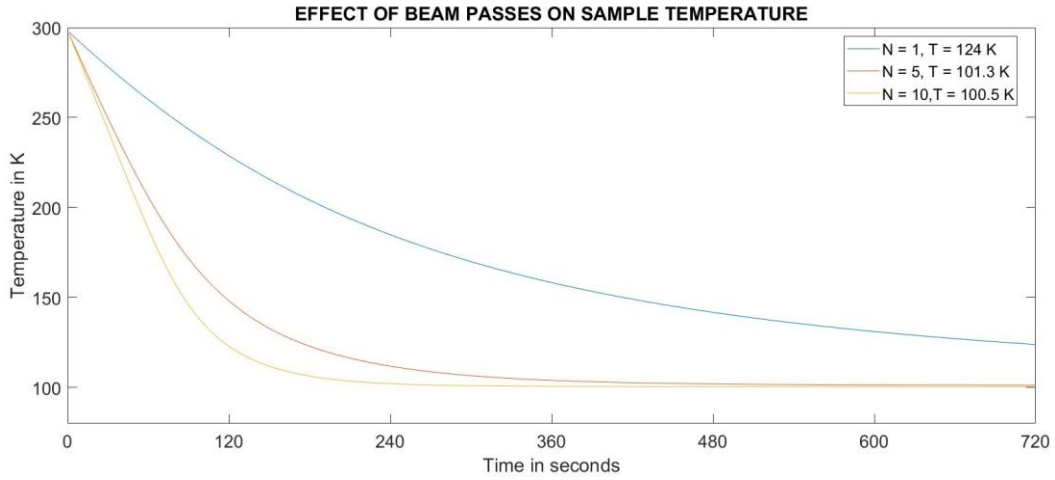

Figure 18 Dynamics of Temperature for multi-pass scheme

As expected improved performance is obtained. The lowest temperature corresponds to 10 beam passes; T = 100.5 K at 12 minutes of operation.

4.3 Solar input to 4-level model

In this section, we explore the effects of utilizing the solar radiation incident on earth surface to pump our optical refrigeration system. As before, we consider a filter which permits only those wavelengths that result in cooling to irradiate our sample whose dimension is unchanged. The goal is to calculate the resulting cooling power and cooling efficiency for the wavelength ranging between 1010 to 1060 nm [48]. The concept is illustrated below:

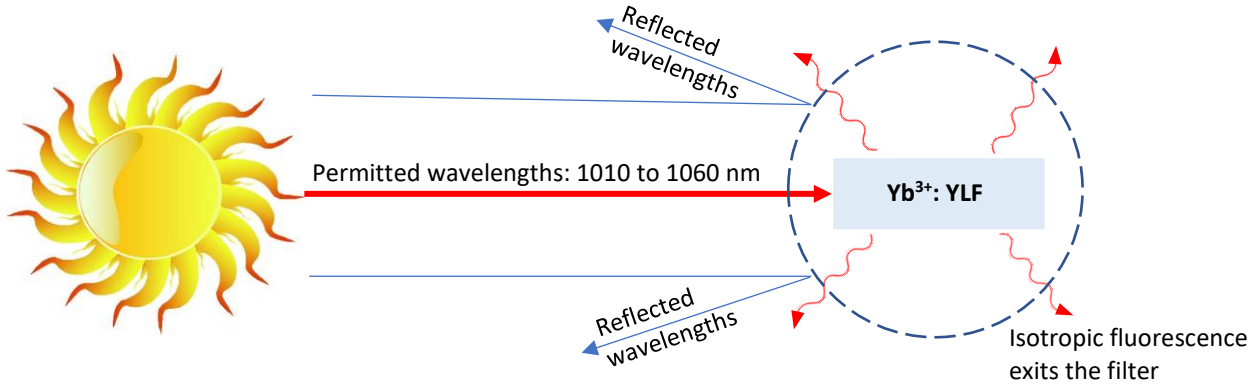

Figure 19 Solar irradiation concept

Using ASTM standard [45] we find the solar spectral irradiance (direct + circumsolar) for 1010 to 1060nm. A graph is plotted in excel using the values in the standard for representation purpose. For better resolution the standard can be referred to. The graph is shown below:

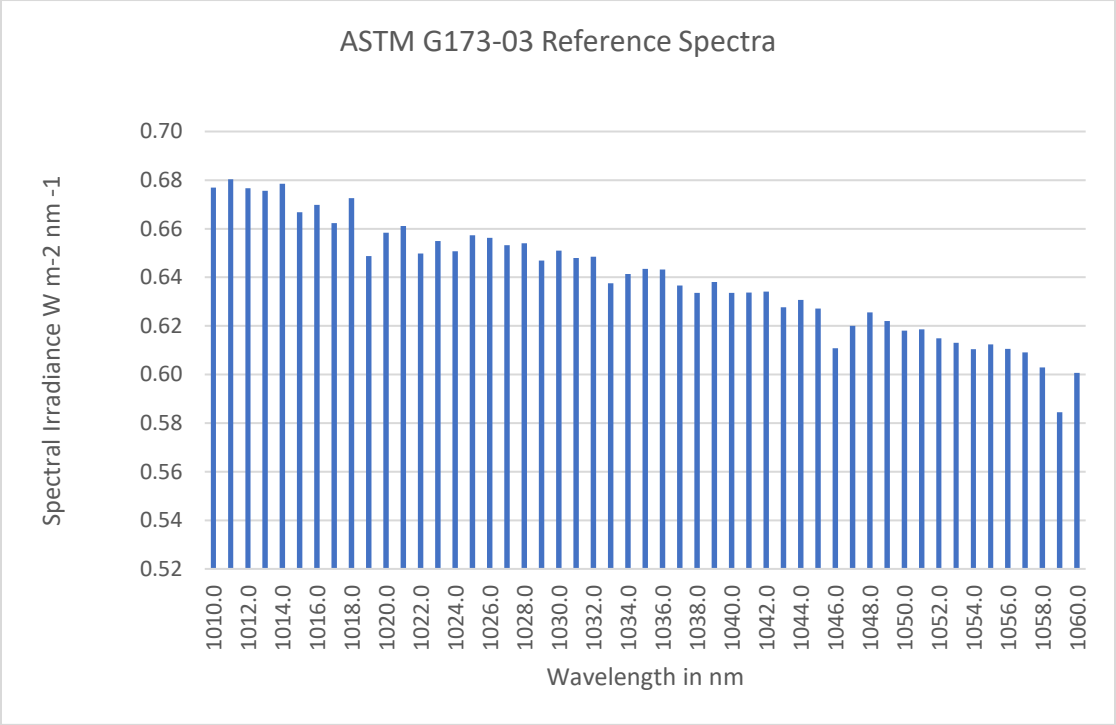

Figure 20 Solar Spectral Irradiance vs Wavelength

For each wavelength in the 1010-1060 nm range, both π, σ polarization emission cross-section is found from *Figure 12* and their average value is found. From this average emission cross-section, the absorption cross-section corresponding to each wavelength in the 1010-1060nm range is calculated by the modified Mc Cumber relation given in Eq.(4.12). From the absorption cross-section, the absorption coefficient, α, is found from Eq.(4.16). The calculated average emission cross-section σ_{21} is represented in the form of a graph below.

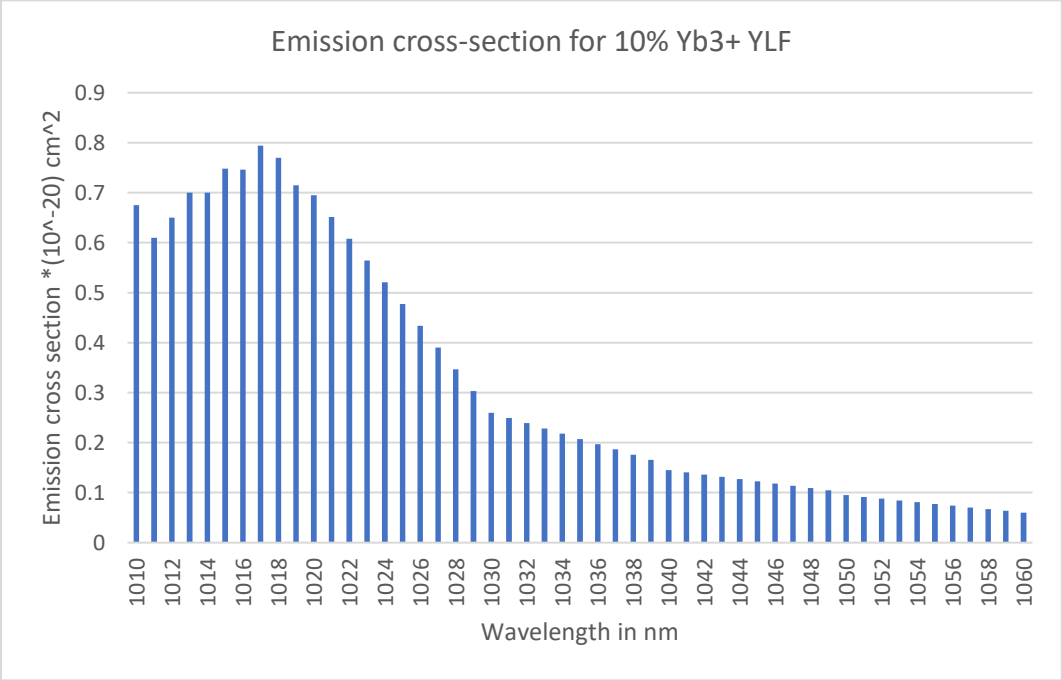

Figure 21 Average emission cross-section for solar irradiance

By feeding α and other relevant parameters to the 4-level model discussed before, the cooling efficiency η_c is found for each wavelength in the 1010-1060 nm range. With the sample dimensions same as before and from the intensity data from Figure 20, the solar power incident on the active material, for each wavelength, is found. Then, Eq.*(4.17*) is used to obtain the cooling power for each pump wavelength, with the number of beam passes assumed to be unity. The above steps are repeated for each wavelength between 1010 to 1060 nm. Then the individual cooling power for each wavelength are added together to result in the net cooling power of the sample by solar irradiation.

Cooling efficiency distribution

The cooling efficiency distributed over the pump wavelengths is shown in Figure 22. The results from MATLAB are plotted using excel. The cooling efficiency is almost constant but for a very small increase from 1010 - 1030 nm. Beyond 1030 nm it starts declining, from 1.95 % at 1030 nm to 1.5% at 1060 nm.

Cooling power distribution

For each wavelength the determined cooling efficiency is utilized to calculate the cooling power. The resulting graph is shown in Figure 23. The total cooling power for solar input is found to be 51.5 µW. The total input solar power from the standard is found to be 7.3 mW.

Cooling efficiency for solar input

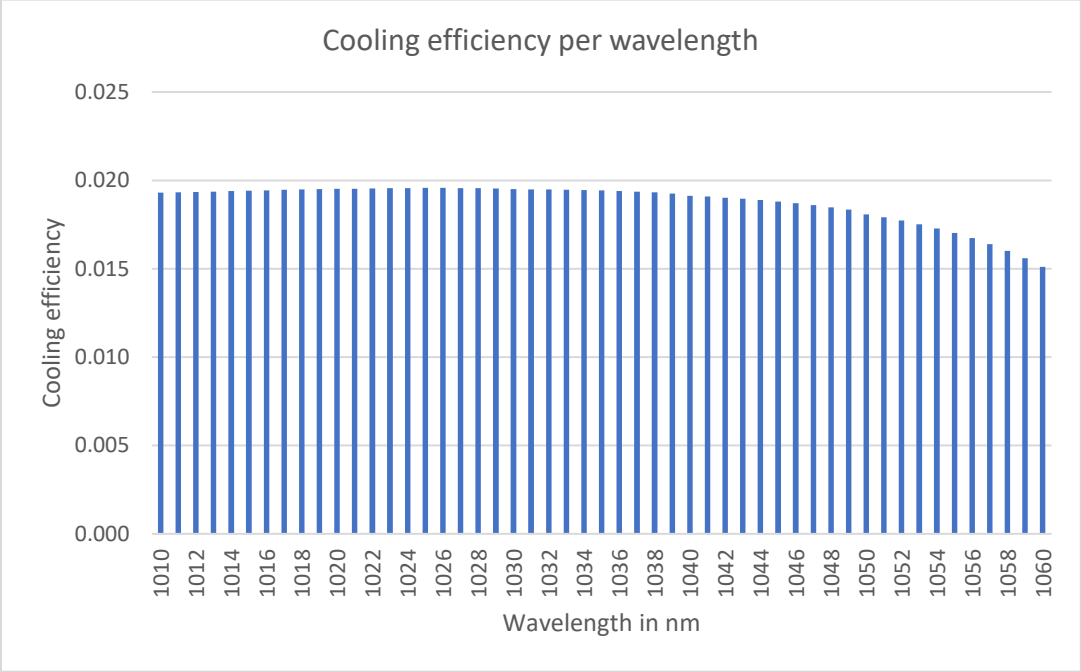

Figure 22 Cooling efficiency per wavelength for solar irradiance

Cooling power for solar input

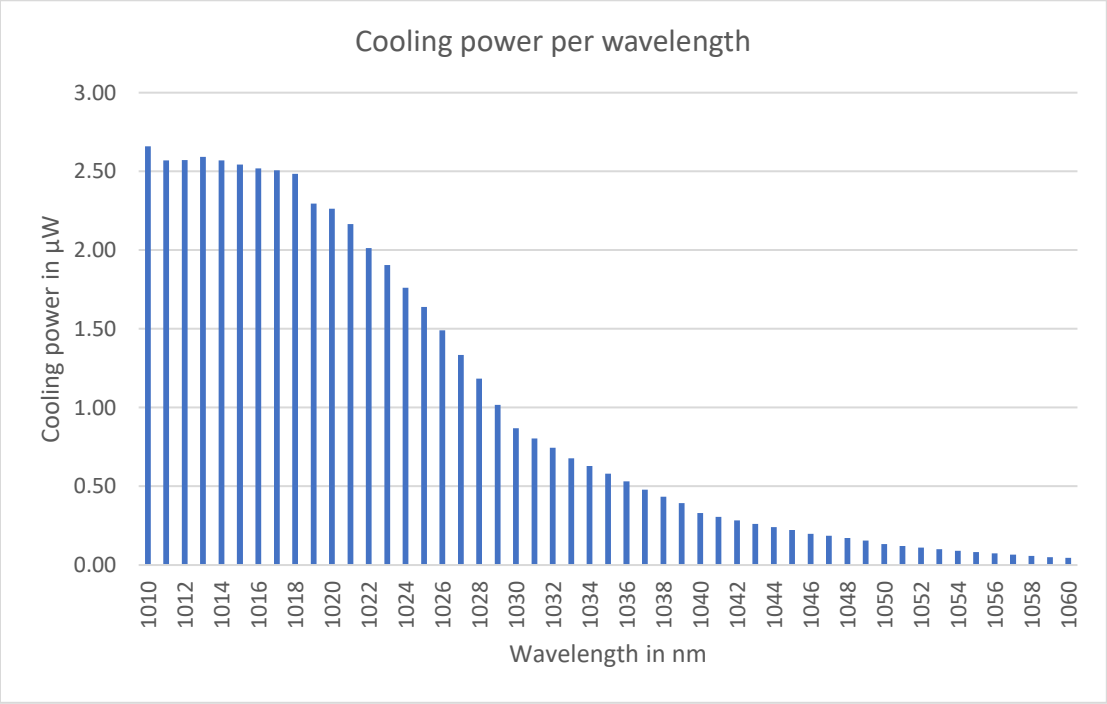

Figure 23 Cooling power per wavelength for solar irradiance

4.4 Fluorescence utilization

Many applications will be possible if the basic efficiency of optical refrigerators can be improved [50]. By harvesting fluorescence power, efficiency can thus be enhanced. One possible way of fluorescence utilization is to capture it with a photo-voltaic system which then feeds electrical power to a laser diode. A schematic of this system is show in the figure below.

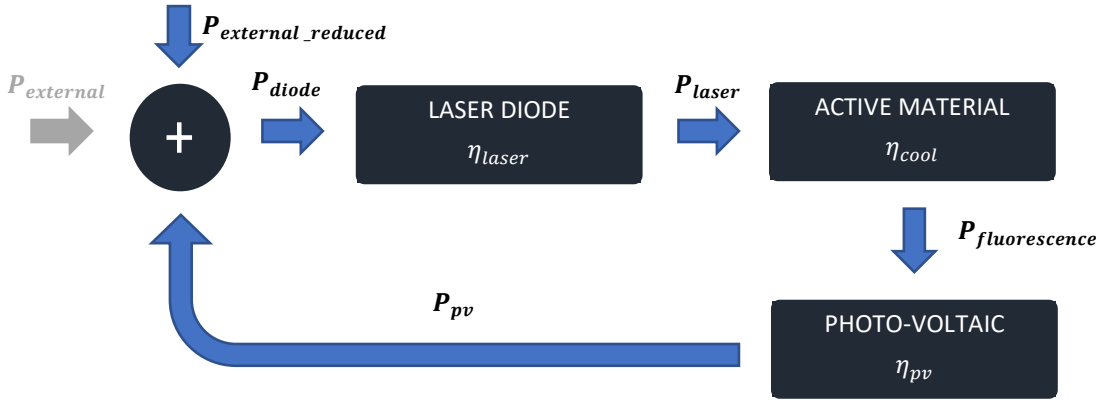

Figure 24 Fluorescence utilization by enhancing electrical efficiency

In the above figure, the arrow shaded with grey represents the required electrical power, $P_{external}$, of the unmodified cooling system (i.e. without fluorescence utilization). With fluorescence utilization $P_{external}$ becomes $P_{external\_reduced}$ highlighting the reduced external electrical power needed for laser operation.

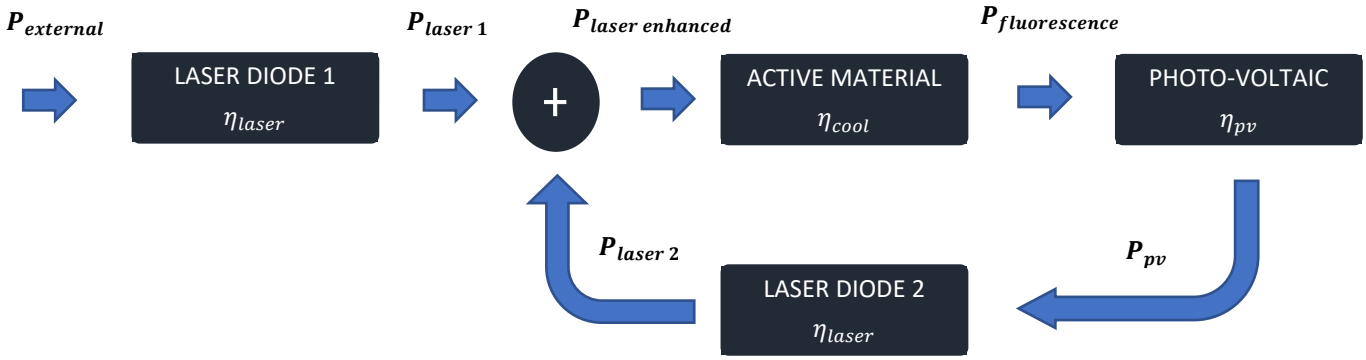

Figure 25 Fluorescence utilization by enhancing cooling power

The above figure shows the possibility of fluorescence utilization wherein, for the same external (electrical) laser power, the cooling power is enhanced by enhanced laser optical power. Another possibility is, for the same cooling power, the required external (electrical) laser power can be reduced.

Both cases have a separate laser diode powered by photovoltaics. Thus, depending on the need the photovoltaic power can be utilized effectively.

Let's assume fluorescence utilization scheme is applied wherein the required laser power is reduced for the same cooling power. Let η_{PV} and η_l represent photo-voltaic and laser efficiency.

Cooling efficiency is expressed as

$$\eta_c = \frac{P_{cool}}{P_{ab}} = \frac{P_{fl} - P_{in} * (1 - e^{-N*\alpha*L})}{P_{in} * (1 - e^{-N*\alpha*L})} \tag{4.18}$$

By fluorescence utilization, for the same cooling power the required laser power is reduced as follows:

$$P_{in\,new} = P_{in} - \eta_{PV} * \eta_l * P_{fl} \tag{4.19}$$

Thus, the new cooling efficiency becomes

$$\eta_{c\,new} = \frac{P_{fl} - P_{in\,new} * (1 - e^{-N*\alpha*L})}{(P_{in} - \eta_{PV} * \eta_l * P_{fl}) * (1 - e^{-N*\alpha*L})} \tag{4.20}$$

Dividing Eq.*(4.20*) by Eq.*(4.18*), we get

$$\frac{\eta_{c\,new}}{\eta_c} = \frac{P_{fl} - P_{in\,new} * (1 - e^{-N*\alpha*L})}{(P_{in} - \eta_{PV} * \eta_l * P_{fl}) * (1 - e^{-N*\alpha*L})} * \frac{P_{in} * (1 - e^{-N*\alpha*L})}{P_{fl} - P_{in} * (1 - e^{-N*\alpha*L})} \tag{4.21}$$

We can re-write Eq.*(4.18*) as:

$$1 + \eta_c = \frac{P_{fl}}{P_{in} * (1 - e^{-N*\alpha*L})} \tag{4.22}$$

By substituting Eq.*(4.22*) into Eq.*(4.21*) and simplifying further we get

$$\frac{\eta_{c\,new}}{\eta_c} = \frac{1}{1 - \eta_{PV} * \eta_l * (1 + \eta_c)} \tag{4.23}$$

Thus, the above equation represents the enhancement factor one can expect in the cooling efficiency by above fluorescence utilization scheme. Choosing present day record laser efficiency of 0.65 [63] and solar photo-voltaic efficiency of 0.35 [64], we get an enhancement factor of 1.3 for the cooling efficiency. This will only rise with future innovations. By engineering photo-voltaic material to effectively capture this ~ 35nm band-gap fluorescence, conversion efficiencies higher than 35 % (solar photo-voltaic conversion efficiency) are possible. This will further boost the enhancement factor.

5. Conclusion

In the present work a comprehensive study on optical refrigeration was performed. The study included theoretical investigations into the material, thermodynamic and quantum-mechanical aspects of the system. The gained knowledge was then applied to analyze novel, unconventional cooling concepts with 10% Yb^{3+}: YLF as the chosen active material. As opposed to the common name "laser cooling" in literature, the present reports title explicitly contains "optical refrigeration" to convey, theoretically, the cooling capabilities of solar radiations.

Based on the analysis carried out in this report, the following conclusions are drawn for 10% Yb^{3+}: YLF

CARNOT EFFICIENCY:

For the same optical power, it was seen that the entropy of diode laser is much less (almost zero) than the entropy of the black-body radiation. Still, the Carnot efficiency of optical refrigeration with laser input is only 10% higher than the one with solar radiation input.

4-LEVEL MODEL, SINGLE PASS:

The following are the results of the simulation based on the 4-level model of optical refrigeration:

- Lowest temperature achieved = 124 K
- Cooling power at ambient = 400 mW
- Cooling power at 124 K = 3.5 mW
- Cooling efficiency at ambient K = 1.9%
- Cooling efficiency at 124 K = 1.4%
- Percentage of laser power absorbed at ambient = 38%
- Percentage of laser power absorbed at 124 K = 2.2%

4-LEVEL MODEL, MULTI PASS:

For 10 passes we obtain the following results:

- Lowest temperature achieved = 100.5 K
- Cooling power at ambient = 1.03 W
- Cooling power at 100.6 K = 3.39 mW
- Cooling efficiency at ambient K = 1.9%
- Cooling efficiency at 100.6 K = 0.1%
- Percentage of laser power absorbed at ambient = 99.19%
- Percentage of laser power absorbed at 106.7K = 6.2%

FLUORESCENCE UTILIZATION:

It was seen that by incorporating photovoltaic capture of the waste fluorescence the cooling efficiency can be enhanced by a factor of 1.3, using today's technology. Designed effectively this system can meet requirements of both light management and energy efficiency.

SOLAR MODEL:

For an input power of 7.3 mW, cooling power of 51.5 μW is obtained. The cooling power can be enhanced by employing schemes to have more round trips of the solar beam within the active material and utilizing a combination of active materials to effectively capture the solar energy.

LOOKING AHEAD:

Further research on both laser and solar based optical refrigeration will be carried out post-graduation and subsequent incubation at YES!Delft as a tech start-up.

6. Recommendations

Absorption co-efficient determination

The lowest achievable temperature of 10% Yb^{3+}: YLF, by laser cooling, was evaluated to be 89K [44]. The researchers reached 91 K after 12 minutes of pumping with the chamber temperature of 265 K and incorporating a 22-pass mechanism of the pump beam. Running a simulation with the above modifications we get a temperature of 99.9 K after 12 minutes of pumping. The result is shown below:

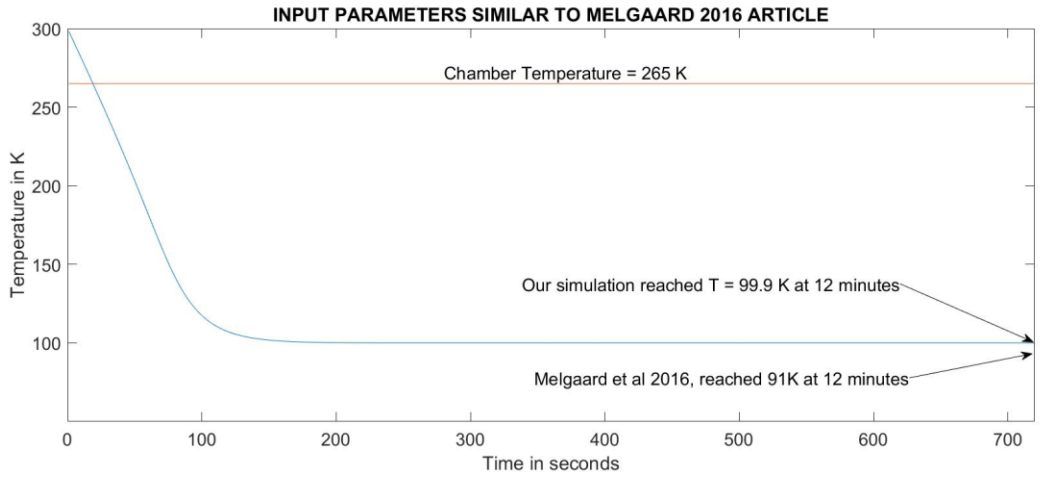

Figure 26 Temperature dynamics with input parameters from Melgaard et al [44]

Melgaard et al [44] article doesn't specify the absorption coefficient value, α, which was identified to be a possible parameter causing the discrepancy in our result. Indeed, after a brief literature review, it was found the absorption coefficient, α , for 10% doped Yb^{3+}:YLF at 300 K is around 1.2 cm^{-1} for an intra-cavity enhanced optical refrigeration [65] whereas the absorption coefficient we obtained was 0.4 cm^{-1}. Although data on the intensity levels utilized in the experiment is not available in the above article, which affects α, further research on the theoretical determination of this value is needed.

This could also mean that the simplification we made in Eq. *(4.13*) wherein we assumed equal degeneracy in all levels might just not be entirely valid. This provides direction for future investigation. Furthermore, in many literatures including Melgaard et al [44] article, the Mc Cumber relation given in Eq.*(4.12*) is modified and is evaluated with an experimental input parameter, by measuring the spectral intensity of emission spectra. It is recommended to experimentally verify the absorption co-efficient.

Heat load determination

The present report can be extended in a relevant direction by incorporating the conduction-based heat transfer mechanism for the case of magnetically suspended platform. For weaker vacuum conditions, the convective heat transfer mechanism should be included as well. It becomes essential to include the conduction-based heat transfer mechanism when the active material is not magnetically suspended and has a thermal contact with the chamber wall. Furthermore, for a multi pass scheme, the amount of light absorbed by the mirrors should also be taken into account as this too will contribute to the heat load input of the optical refrigerator.

Light management

It's important that the emitted fluorescence leaves the sample space without re-absorption by the active material or by a thermal link which has contact with the active material. One possibility for a magnetically suspended platform is to use mirrored surfaces, with the mirror panels arranged in a particular fashion such that the incident fluorescence gets deflected directly to the chamber walls. The concept is shown in dotted line in the below figure, which also contains the heat load balance of the magnetically suspended optical refrigerator.

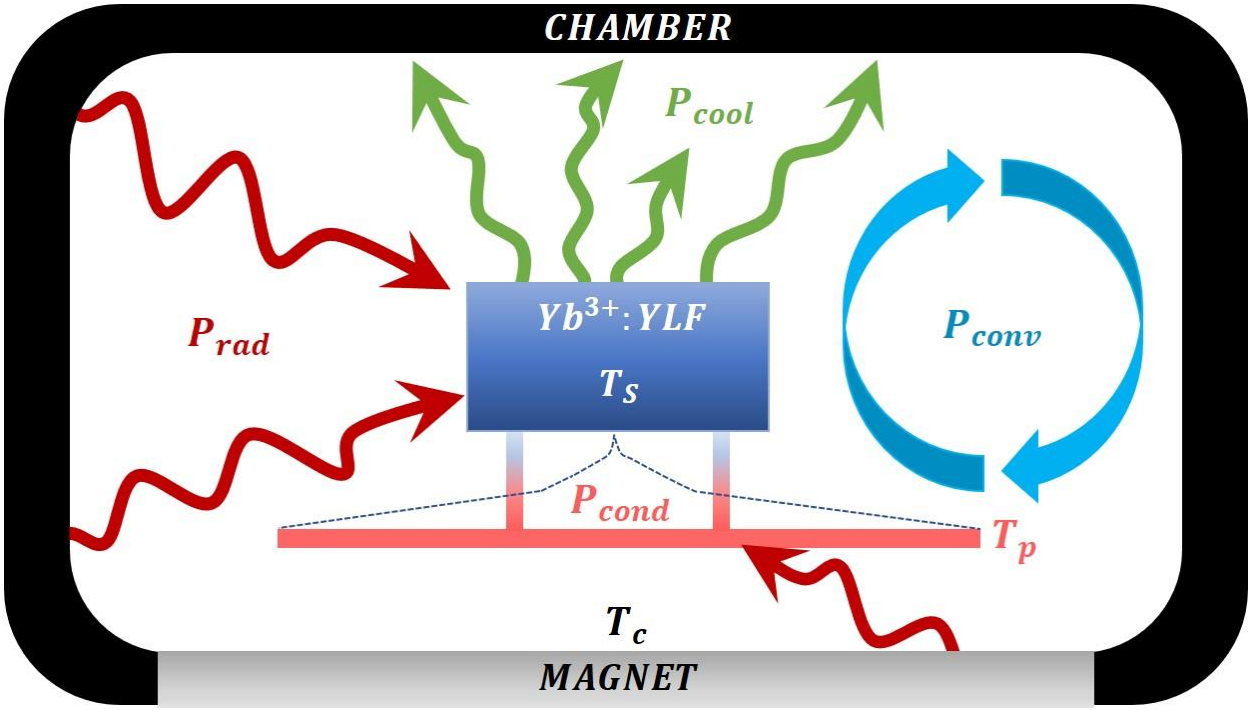

Figure 27 Heat load model

Active material selection

Active material selection should be done on the basis of the application. For instance, Ytterbium doped in YAG has almost double the thermal conductivity of the YLF host and thus might be better suitable for thermal management applications requiring larger heat lifts. Cadmium Sulfide is a very attractive candidate for optical refrigeration as it's cooling power density is six times higher than the rare-earth doped glassy/crystal hosts. However, it's MSDS (Material Safety Data Sheet) should be referred before considering an application as it appears to have carcinogenic (cancer-causing) effects.

7. Bibliography

[1] D. V. Seletskiy, R. I. Epstein and M. . Sheik-Bahae, "Laser cooling in solids: advances and prospects," *Reports on Progress in Physics,* vol. 79, no. 9, p. 096401, 2016.

[2] S. Chu, "Steven Chu - Nobel Lecture," *Nobel Lectures, Physics 1996-2000,* vol. , no. , p. 122, .

[3] G. Nemova, "Laser cooling in rare earth doped glasses and crystals," in *Laser cooling: fundamental properties and application*, 2016, pp. 37 - 82.

[4] P. Pringsheim, "Zwei Bemerkungen über den Unterschied von Lumineszenz- und Temperaturstrahlung," *Zeitschrift für Physik,* vol. 57, no. 11-12, p. 739–746, 1929.

[5] G. G. Stokes, "On the Change of Refrangibility of Light," *Philosophical Transactions of the Royal Society of London,* vol. 142, no. , p. 463–562, 1852.

[6] S. Vavilov, "Photoluminescence and thermodynamics,," *J. Phys. (Moscow) 10,* p. 499–501 , 1946.

[7] L. Landau, "On the thermodynamics of photoluminescence," *J. Phys. (Moscow) 10,* p. 503–506, 1946.

[8] A. Rayner, N. R. Heckenberg and H. . Rubinsztein-Dunlop, "Condensed-phase optical refrigeration," *Journal of The Optical Society of America B-optical Physics,* vol. 20, no. 5, pp. 1037-1053, 2003.

[9] S.Varilov, "Some remarks on the Stokes law," *J.Phys (Moscow),* vol. 9, pp. 68-73, 1945.

[10] R. I. Epstein, "Observation of laser-induced flourescent cooling of a solid," *Nature,* vol. 377, pp. 500-503, 1995.

[11] M. Sheik-Bahae and R. I. Epstein, "Laser cooling of solids," *Laser & Photonics Reviews,* vol. 3, no. , pp. 67-84, 2009.

[12] A.Kastler, *J.Phys.Radium,* vol. 11, pp. 255-265, 1950.

[13] S.Yatsiv, "Anti-Stokes fluorescence as a cooling process," *Advances in Quantum electronics,* pp. 200-213, 1961.

[14] E. Geusic, "Optical refrigeration in Nddoped yttrium aluminum garnet,," *Phys.Rev.Lett.21,* pp. 1172-1175, 1968.

[15] T. R. Gosnell, "Laser cooling of a solid by 65 K starting from room temperature," *Optics Letters,* vol. 23, no. 8, pp. 1041-1043, 1998.

[16] M. P. Hehlen, "Novel materials for laser refrigeration," , 2009. [Online]. Available: https://spiedigitallibrary.org/redirect/proceedings/proceeding?doi=10.1117/12.809091. [Accessed 6 3 2018].

[17] S. Hufner, Optical spectra of transparent rare-earth compounds, New York, 1978.

[18] L. A. Riseberg, H. W. Moos and W. D. Partlow, "Multiphonon relaxation in laser materials and applications to the design of quantum electronic devices," *IEEE Journal of Quantum Electronics,* vol. 4, no. 10, pp. 609-612, 1968.

[19] J.M.F. van Dijk, "On the nomadiative and radiative decay rates and a modified exponential energy gap law for 4f-4f transitions in rare-earth ions," *J.Chem. Phys,* vol. 78, 1983.

[20] M.P. Hehlen, "Model of laser cooling in the Yb3+-doped fluorozirconate glass ZBLAN," *Phys.Rev.B,* 2007.

[21] G.Z. Dong, X. Zhang and L. Li, "Energy transfer enhanced laser cooling in Ho 3+ and Tm 3+ - codoped lithium yttrium fluoride," *Journal of The Optical Society of America B-optical Physics,* vol. 30, no. 4, pp. 939-944, 2013.

[22] P. B. Roder, B. E. Smith, X. . Zhou, M. J. Crane and P. J. Pauzauskie, "Laser refrigeration of hydrothermal nanocrystals in physiological media," *Proceedings of the National Academy of Sciences of the United States of America,* vol. 112, no. 49, pp. 15024-15029, 2015.

[23] C. W. Hoyt, M. P. Hasselbeck, M. . Sheik-Bahae, R. I. Epstein, S. R. Greenfield, J. . Thiede, J. . Distel and J. . Valencia, "Advances in laser cooling of thulium-doped glass," *Journal of The Optical Society of America B-optical Physics,* vol. 20, no. 5, pp. 1066-1074, 2003.

[24] S. Eshlaghi, W. A. Worthoff, A. D. Wieck and D. . Suter, "Luminescence upconversion in GaAs quantum wells," *Physical Review B,* vol. 77, no. 24, p. 245317, 2008.

[25] M. Sheik-Bahae and R. I. Epstein, "Optical refrigeration," *Nat.Photon,* vol. 12, 2007.

[26] A. Gauck, "External radiative quantum efficiency of 96% from a GaAs/GaInP heterostructure," *Appl.Phys.,* pp. 142-147, 1997.

[27] J. Zhang, D. Li, R . Chen and Q . Xiong, "Laser cooling of a semiconductor by 40 kelvin," *Nature,* vol. 493, no. 7433, pp. 504-508, 2013.

[28] M. Sheik-Bahae and R. I. Epstein, "Can laser light cool semiconductors?," *Phys.Rev.Lett,* vol. 92, 2004.

[29] J. B. Khurgin, "Band gap engineering for laser cooling of semiconductors," *Journal of Applied Physics,* vol. 100, no. 11, p. 113116, 2006.

[30] J. B. Khurgin, "Role ofbandtail states in laser cooling of semiconductors," *Phys.Rev.B,* vol. 77, 2008.

[31] Q. Xiong, "Laser Cooling of II-VI Semiconductors," NANYANG TECHNOLOGICAL UNIVERSITY, Singapore, 2016.

[32] S. T. Ha, C. Shen, J . Zhang and Q. Xiong, "Laser cooling of organic–inorganic lead halide perovskites," *Nature Photonics,* vol. 10, no. 2, pp. 115-121, 2016.

[33] Q. Dong, Y. Fang, Y. Shao, P. Mulligan, J. Qiu, L. Cao and J. Huang, "Electron-hole diffusion lengths >175 μm in solution grown CH3NH3PbI3 single crystals," *Science,* vol. 347, no. 6225, pp. 967-970, 2015.

[34] D. Shi, "Low trap-state density and long carrier diffusion in organolead trihalide perovskite single crystals," *Science,* pp. 967-970, 2015.

[35] H. L. M. Wehrenfennig, "High charge carrier mobilities and lifetimes in organolead trihalide perovskites," *Adv. Mater.,* vol. 26, pp. 1584-1589, 2014.

[36] X. Ruan, S. C. Rand and M. Kaviany, "Entropy and efficiency in laser cooling of solids," *Physical Review B,* vol. 75, no. 21, p. , 2007.

[37] H. E. D. Scovil and E. O. Schulz-DuBois, "Laser cooling by spontaneous anti-Stokes scattering," *Phys. Rev. Lett,* vol. 2, p. 262–263, 1959.

[38] J. E. Geusic, "Quantum equivalent of the carnot cycle,," *Phys. Rev,* vol. 156, pp. 343-351, 1967.

[39] M. A. Weinstein, "Thermodynamic Limitation on the Conversion of Heat into Light," *Journal of the Optical Society of America,* vol. 50, no. 6, pp. 597-602, 1960.

[40] T. R. Gosnell, "Laser cooling of solids," *Adv. At., Mol., Opt. Phys,* vol. 40, pp. 161-228, 1999.

[41] X. Ruan, S. C. Rand and M . Kaviany, "Entropy and efficiency in laser cooling of solids," , 2007. [Online]. Available: http://proceedings.asmedigitalcollection.asme.org/proceeding.aspx?articleid=1590540. [Accessed 31 5 2018].

[42] C. E. Mungan, "Radiation thermodynamics with applications to lasing and fluorescent cooling," *American Journal of Physics,* vol. 73, no. 4, pp. 315-322, 2005.

[43] P. T. Landsberg and G. . Tonge, "Thermodynamic energy conversion efficiencies," *Journal of Applied Physics,* vol. 51, no. 7, p. , 1980.

[44] S. D. Melgaard, A. R. Albrecht, M. P. Hehlen and M. . Sheik-Bahae, "Solid-state optical refrigeration to sub-100 Kelvin regime.," *Scientific Reports,* vol. 6, no. 1, p. 20380, 2016.

[45] ASTM, "Reference Solar Spectral Irradiance: ASTM G-173," ASTM International, 2003. [Online]. Available: http://rredc.nrel.gov/solar/spectra/am1.5/astmg173/astmg173.html.

[46] S. D. Melgaard, "Cryogenic optical refrigeration: Laser cooling of solids below 123 K," , 2013. [Online]. Available: http://repository.unm.edu/handle/1928/23136. [Accessed 7 6 2018].

[47] D. V. Seletskiy, R. I. Epstein and M. . Sheik-Bahae, "Laser cooling in solids: advances and prospects," *Reports on Progress in Physics,* vol. 79, no. 9, p. 096401, 2016.

[48] S. D. Melgaard, D. V. Seletskiy, A. D. Lieto, M. . Tonelli and M. . Sheik-Bahae, "Optical refrigeration progress: cooling below NIST cryogenic temperature of 123K," *Proceedings of SPIE,* vol. 8638, no. , p. 863804, 2013.

[49] W. S. Warren, The Physical Basis of Chemistry, 2000.

[50] M. S.-B. a. R. I. Epstein, "Laser cooling of solids," *Laser and Photonics Review,* vol. 3, no. 1-2, pp. 67-84, 2009.

[51] A. Bensalah, "Growth of Yb3+doped YLiF4 laser crystal by the Czochralski method. Attempt of Yb3+ energy level assignment and estimation of the laser potentiality," *Optical Materials 26,* pp. 375-383, 2004.

[52] D. McCumber, "EINSTEIN RELATIONS CONNECTING BROADBAND EMISSION AND ABSORPTION SPECTRA," *Physical Review,* vol. 136, no. , p. , 1964.

[53] L. D. DeLoach, S. A. Payne, L. L. Chase, L. K. Smith, W. L. Kway and W. F. Krupke, "Evaluation of absorption and emission properties of Yb/sup 3+/ doped crystals for laser applications," *IEEE Journal of Quantum Electronics,* vol. 29, no. 4, pp. 1179-1191, 1993.

[54] S. D. Melgaard, "Cryogenic optical refrigeration: Laser cooling of solids below 123 K," Univ. of New Mexico, New Mexico, 2013.

[55] M. A. Rahman, "Laser refrigeration, alignment and rotation of levitated Yb3+:YLF nanocrystals," *Nature Photonics,* vol. 11, pp. 634-638, October 2017.

[56] Denis V. Seletskiy, "Precise determination of minimum achievable temperature for solid-state optical refrigeration," *J. Lumin,* 2012.

[57] A. Volpi, A. D. Lieto and M. . Tonelli, "Novel approach for solid state cryocoolers.," *Optics Express,* vol. 23, no. 7, pp. 8216-8226, 2015.

[58] P. B. Roder, B. E. Smith, X. . Zhou, M. J. Crane and P. J. Pauzauskie, "Laser refrigeration of hydrothermal nanocrystals in physiological media," *Proceedings of the National Academy of Sciences of the United States of America,* vol. 112, no. 49, pp. 15024-15029, 2015.

[59] R. L. Aggarwal, "Measurement of thermo-optic properties of Y3Al5O12, Lu3Al5O12, YAIO3, LiYF4, LiLuF4, BaY2F8, KGd„WO4…2, and KY„WO4…2 laser crystals in the 80–300 K temperature range," *JOURNAL OF APPLIED PHYSICS,* vol. 98, 2005.

[60] D. V. Seletskiy, M. P. Hehlen, R. I. Epstein and M. . Sheik-Bahae, "Cryogenic optical refrigeration," *Advances in Optics and Photonics,* vol. 4, no. 1, pp. 78-107, 2012.

[61] B. C. Edwards, J. E. Anderson, R. I. Epstein, G. L. Mills and A. J. Mord, "Demonstration of a solid-state optical cooler: An approach to cryogenic refrigeration," *Journal of Applied Physics,* vol. 86, no. 11, pp. 6489-6493, 1999.

[62] C. Hoyt, "Laser cooling in thulium-doped solids," University of New Mexico, New Mexico, 2003.

[63] E. T. Alexei Baranov, "High power semiconductor laser," in *Semiconductor Lasers: Fundamentals and Applications*, 2013, p. 84.

[64] P. Europe, "PV Europe," 2017. [Online]. Available: http://www.pveurope.eu/News/Solar-Generator/Record-solar-cell-with-35.9-percent-efficiency.

[65] M. Ghasemkhani, A. R. Albrecht, S. D. Melgaard, D. V. Seletskiy, J. G. Cedeberg and M. . Sheik-Bahae, "Intracavity optical refrigeration to 131K using high-power vertical external-cavity surface-emitting lasers (VECSELs)," *Proceedings of SPIE,* vol. 9000, no. , p. 900005, 2014.

[66] P. Pringsheim, "Some remarks concerning the difference between luminescence and temperature radiation, Anti-Stokes fluorescence," *J. Phys. (Moscow) 10,* p. 495–498, 1946.

[67] M. Melgaard, "First solid-state cooling below 100 K,," *SPIE Newsroom,* 2015.

[68] B. C. Edwards, J. E. Anderson, R. I. Epstein, G. L. Mills and A. J. Mord, "Demonstration of a solid-state optical cooler: An approach to cryogenic refrigeration," *Journal of Applied Physics,* vol. 86, no. 11, pp. 6489-6493, 1999.

[69] J. Thiede, "Cooling to 208 K by optical refrigeration,," *Appl.Phys.Lett,* vol. 86, no. 15, 2005.

[70] R. I. Epstein, J. J. Brown, B. C. Edwards and A. . Gibbs, "Measurements of optical refrigeration in ytterbium-doped crystals," *Journal of Applied Physics,* vol. 90, no. 9, pp. 4815-4819, 2001.

[71] A. Bigotta, "Spectroscopic and laser cooling results on Yb3+-doped BaY2F8 single crystal," *J.Apply.Phys,* vol. 100, no. 1, 2006.

[72] W. Patterson, S. Bigotta, M. Sheik-Bahae, D. Parisi, M. Tonelli and R. I. Epstein, "Anti-Stokes luminescence cooling of Tm3+ doped BaY2F8.," *Optics Express,* vol. 16, no. 3, pp. 1704-1710, 2008.

[73] B. R. Fernandez, "Anti-Stokes Laser Cooling in Bulk Erbium-Doped Materials," *Phys.Rev.Lett.,* vol. 97, no. 3, 2006.

[74] B. R. Fernandez, "Anti-Stokes laser-induced cooling in rare-earth doped low phonon materials," *Opt.Mater.,* vol. 34, no. 3, 2012.

[75] L. Filho, G. Nemova, S. Loranger and R. Kashyap, "Laser-induced cooling of a Yb:YAG crystal in air at atmospheric pressure.," *Optics Express,* vol. 21, no. 21, pp. 24711-24720, 2013.

[76] M. V. Ter, "Optical Properties and Optical Spectroscopy of Rare Earth Ions in Solids," in *Fundamentals of Fiber Lasers and Fiber Amplifiers*, Mountain View USA, Springer, Cham, November 2013, pp. 7-26.

[77] J.-F. Seurin, C. Ghosh, V. Khalfin, A. Miglo, G. Xu, J. D. Wynn, P. Pradhan and L. A. D'Asaro, "High-power high-efficiency 2D VCSEL arrays," , 2008. [Online]. Available: https://spiedigitallibrary.org/conference-proceedings-of-spie/6908/1/high-power-high-efficiency-2d-vcsel-arrays/10.1117/12.774126.full. [Accessed 8 6 2018].

[78] B. S. Lab, "photovoltaics," Spectro Lab, 2018. [Online]. Available: https://www.spectrolab.com/solarcells.htm. [Accessed 2018].